REVIEW SUMMARY

NANOMATERIALS

The world of two-dimensional carbides and nitrides (MXenes)

Armin VahidMohammadi, Johanna Rosen, Yury Gogotsi*

BACKGROUND: Appreciation of the fact that synthesis of two-dimensional (2D) materials does not necessarily require van der Waals bonded layered precursors led to discovery of many new materials, including MXenes-2D carbides and nitrides of transition metals, produced by selective etching of strongly bonded layered solids. Ti_3C_2 was first reported in 2011 and set the stage for synthesis of Ti₂C, Ta₄C₃, and other MXenes from their MAX phase precursors, demonstrating three types of possible structures (M_2X , M_3X_2 , and M_4X_3). M_5C_4 was later produced, further increasing the structural diversity and bringing the number of theoretically possible compositions to more than 100, including those with in-plane and out-of-plane ordering of the metal atoms. Con-

sidering various surface terminations of MXenes, the number of distinct compositions increases by another order of magnitude. The ability of MXenes to form carbonitrides and solid solutions suggests a potentially infinite number of compositions and opens a new era of computationally driven atomistic design of 2D materials.

ADVANCES: MXenes add a large number of building blocks, mainly metallic conductors, to the family of 2D materials, most of which are dielectrics, semiconductors, or semimetals. By using tunable properties of MXenes, one can build devices ranging from transistors to supercapacitors, batteries, antennas, and sensors from 2D nanosheets by using additive manufacturing or other coating and process-

Energy storage nterference shielding 2D MXenes Environmental **Biomedicine Optoelectronics**

Structure and applications of 2D carbides and nitrides (MXenes). The large number of MXene compositions having structures with three, five, seven, or nine atomic layers containing one or two kinds of metal atoms and various surface terminations (-F, =0, -Cl, -Br, etc.) have shown promising optoelectronic, mechanical, and electrochemical properties. They have found use in a wide range of applications ranging from energy storage and harvesting to catalysis, water purification and desalination, electromagnetic interference shielding, communication, optics, electronics, plasmonics, sensors, actuators, composites, and medicine.

ing techniques. MXenes have already shown a variety of electronic, optical, chemical, and mechanical properties, and the concept of MXetronics (all-MXene optoelectronics) has been proposed. High electronic conductivity allows their use in current collectors, interconnects, and conductive inks. MXenes possess electrochemically and chemically tunable plasmonic properties, with interband transitions and plasmon resonance peaks covering the entire ultraviolet, visible, and near-infrared range, which allow their electrochromic and photothermal therapy applications. Their strong interaction with electromagnetic waves from terahertz to gigahertz frequencies is used in electromagnetic interference shielding and communication. Redox activity of transition metal atoms on the MXene surface enables electrochemical energy storage in batteries and supercapacitors as well as electrocatalysis. Controlled spacing between the 2D sheets is used for separation of gases, water purification, and dialysis. The surface charge of MXenes allows aqueous processing without surfactants or binders as well as formation of liquid crystals. Organic molecules, polymers, and ions can be intercalated between MXene layers, allowing properties tuning and multilayer assemblies. Nontoxic and environmentally friendly titanium-based MXenes, built of abundant elements, and their hybrids and composites with polymers, ceramics, and metals are particularly attracting considerable attention.

OUTLOOK: While progress has been made on the preparation of carbide MXenes, synthesis of nitrides is trailing behind. Vapor phase synthesis is needed for integration of MXenes on chips using current microfabrication device technology. Large-scale, environmentally friendly synthesis methods are the key to wide use of MXenes in future additive manufacturing technologies. Precise control of the structure and surface chemistry, including defects and strain engineering, should pave the way to theoretically predicted intrinsically semiconducting, topologically insulating, and ferromagnetic MXenes as well as other discoveries in MXene physics and chemistry. Mechanically strong, environmentally stable, and highly conductive MXenes may have a major impact on flexible, printable, and wearable self-powered electronics. However, the use of MXenes in combination with other 2D materials to build heterostructures and devices by self-assembly from solution is perhaps the most exciting prospect. ■

The list of author affiliations is available in the full article online. *Corresponding author, Email: gogotsi@drexel.edu Cite this article as A. VahidMohammadi et al., Science 372, eabf1581 (2021). DOI: 10.1126/science.abf1581



READ THE FULL ARTICLE AT

REVIEW

NANOMATERIALS

The world of two-dimensional carbides and nitrides (MXenes)

Armin VahidMohammadi¹, Johanna Rosen², Yury Gogotsi¹*

A decade after the first report, the family of two-dimensional (2D) carbides and nitrides (MXenes) includes structures with three, five, seven, or nine layers of atoms in an ordered or solid solution form. Dozens of MXene compositions have been produced, resulting in MXenes with mixed surface terminations. MXenes have shown useful and tunable electronic, optical, mechanical, and electrochemical properties, leading to applications ranging from optoelectronics, electromagnetic interference shielding, and wireless antennas to energy storage, catalysis, sensing, and medicine. Here we present a forward-looking review of the field of MXenes. We discuss the challenges to be addressed and outline research directions that will deepen the fundamental understanding of the properties of MXenes and enable their hybridization with other 2D materials in various emerging technologies.

Xenes are a large family of twodimensional (2D) metal carbides and nitrides having a structure consisting of two or more layers of transition metal (M) atoms packed into a honeycomb-like 2D lattice that are intervened by carbon and/or nitrogen layers (X atoms) occupying the octahedral sites between the adjacent transition metal layers (1, 2). MXenes are produced through a top-down synthesis approach, where typically A-layer atoms (e.g., Al, Si, Ga) are selectively removed from the structure of MAX phases, a group of layered, hexagonal-structure ternary carbides and nitrides (3), leaving behind loosely stacked MX layers [called "MXene" to emphasize their 2D nature (2)], which can be further separated into single-layer flakes (Fig. 1).

 $Ti_3C_2T_x$ was made by selective etching of monoatomic Al layers from the Ti₂AlC₂ MAX phase precursor in hydrofluoric (HF) acid (1). High metallic conductivity, hydrophilicity, and the ability to intercalate cations and store charge, demonstrated by $Ti_3C_2T_x$ (4, 5) and other MXenes (6, 7), initially led to interest in exploring MXenes for energy storage applications. The year 2017 was the beginning of the MXenes "gold rush." Since then, the world of 2D carbides and nitrides has been growing at an unprecedented rate. There are currently more than 30 different experimentally made stoichiometric MXenes and more than a hundred (not considering surface terminations) theoretically predicted MXenes (8-10) with distinct electronic, physical, and (electro)chemical properties. In addition, solid

¹A.J. Drexel Nanomaterials Institute and Department of Materials Science and Engineering, Drexel University, Philadelphia, PA 19104, USA. ²Department of Physics, Chemistry, and Biology (IFM), Linköping University, Linköping SE-583 31, Sweden. solutions on M and X sides are possible, and the possibility of having multiple single (O, Cl, F, S, etc.) or mixed (O/OH/F) surface terminations makes MXenes a large and diverse family of 2D materials.

The variety of MXene structures and compositions (Fig. 1) makes it necessary to define a terminology for MXenes. The general formula of MXenes is $M_{n+1}X_nT_x$, where M represents the transition metal site, X represents carbon or nitrogen sites, n can vary from 1 to 4, and T_x (where x is variable) indicates surface terminations on the surface of the outer transition metal layers (8, 11). As an example, the chemical formula of a titanium carbide MXene with two layers of transition metal (n = 1) and random terminations would be Ti₂CT_x, and a completely oxygen- or chlorine-terminated Ti_2CT_x can be written as Ti₂CO₂ or Ti₂CCl₂, respectively. If there are two randomly distributed transition metals occupying M sites in the MXene structure forming a solid solution, the formula will be written as $(M',M'')_{n+1}X_nT_{x}$ where M' and M" are two different metals [e.g., $(Ti,V)_2CT_x$]. For a specific metal composition, the concentration of each element is given in decimal numbers [e.g., $(Ti_{0.66}V_{0.34})_2CT_x$]. If the two metals have in-plane ordering and form alternating chains of M' and M" atoms within the same M layer, the resulting MXene structure is called i-MXene. All i-MXenes known to date have a formula of (M'4/3M"2/3)XT2, where the concentration of each element is given as a fractional number. In most i-MXenes, the M" atoms can be selectively etched, creating ordered vacancies and producing an i-MXene with a formula of $M'_{4/3}XT_x$, previously referred to as M'_{1,33}XT_x. M' and M" atoms can also be located in separate atomic planes having an out-of-plane ordering, called o-MXenes, in which M" atoms constitute the inner metal layers, and M' atoms are placed in the outer layers. o-MXenes are so far known by two formulas, $(M'_2M'')X_2T_x$ and $(M'_2M''_2)X_3T_x$. In addition, all MXenes can either be produced in the form of multilayer particles (ml-MXene) or delaminated (d-MXene) single-layer flakes.

Structure and composition of MXenes

Figure 1 schematically shows the known structures of MXenes. Similar to the basal planes in the MAX phases, MXenes have a hexagonal close-packed (hcp) crystal structure with a $P6_3/mmc$ space group symmetry, where the transition metals in the M sites are close-packed, and the X atoms occupy the octahedral sites in between the M atomic planes (II). MXenes with Ti, V, Nb, Mo, Cr, Zr, Hf, Sc, Ta, W, and Y in the M site have been reported. Note that Cr, Sc, W, or Y have only been reported as components of o-MXenes or i-MXenes, along with other metals mentioned above.

At least 26 different o-MXenes have been theoretically predicted (12), among which Mo₂TiC₂T₂₂ $Mo_2ScC_2T_x$, $Cr_2TiC_2T_x$, and $Mo_2Ti_2C_3T_x$ have already been experimentally reported (13, 14). The ideal o-MXene composition has a ratio of M' to M" of 2:1 or 2:2, originating from the corresponding ratios of different metal lattice sites in the MXene structure. i-MXenes, on the other hand, are favored only when the ratio of M' to M" is 2:1 and the size difference between M" and M' is at least 0.2 Å (15, 16). This requirement originates from the hexagonal atomic arrangement within the M layer, in which the M' atoms form a honeycomb lattice and the M" atoms occupy the hexagon centers and extend out from the M layers (toward the A-layer positions in their parent i-MAX phase) (15). Such atomic arrangement gives i-MAX phases a monoclinic (C2/c) or orthorhombic (C2/m or Cmcm)structure, inherited by i-MXenes (16, 17). So far, 32 different i-MAX phases have been synthesized (12, 18). However, both A and M" elements are simultaneously etched away from most i-MAX phases (18). For example, using HF, both Al and Sc or Y were selectively removed from $(W_{2/3}Sc_{1/3})_2AlC$ and $(W_{2/3}Y_{1/3})_2AlC$, resulting in $W_{1.33}CT_x$ *i*-MXene with ordered divacancies (19). This behavior originates from a weaker bonding of M" elements to the carbon sites, as evidenced by their outward displacement from the M plane (20). These structural characteristics also allow the concept of targeted etching, where tuned synthesis conditions can facilitate removal of either A alone or both the A and M" elements from the i-MAX phase, as shown for Mo_{4/3}Y_{2/3}AlC (20).

The X sites can be occupied by carbon, nitrogen, or both (11). Research on nitride MXenes has been limited, with the exception of ml- Ti_2NT_x and ml- $\text{Ti}_4\text{N}_3\text{T}_x$ (21–23), as the synthesis of nitride MXenes presents a challenge. In carbonitride MXenes, it is believed that the C and N atoms occupy the octahedral sites randomly, independent of carbonitride stoichiometry (8).

^{*}Corresponding author. Email: gogotsi@drexel.edu

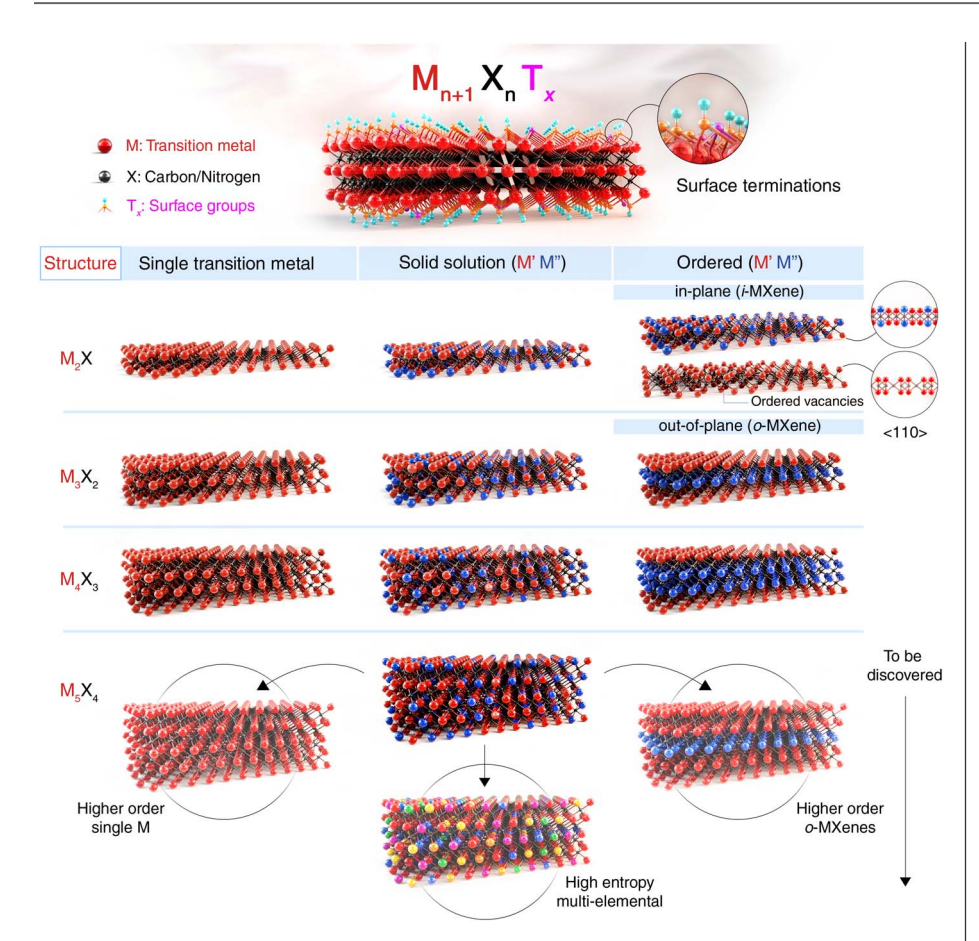


Fig. 1. Schematic illustration of the MXene structures. 2D MXenes have a general formula of $M_{n+1}X_nT_x$, where M is an early transition metal, X is carbon and/or nitrogen, and T_x represents surface terminations of the outer metal layers. The n value in the formula can vary from 1 to 4, depending on the number of transition metal layers (and carbon and/or nitrogen layers) present in the structure of MXenes, for example, $T_{12}CT_x$ (n=1), $T_{13}C_2T_x$ (n=2), $Nb_4C_3T_x$ (n=3), and $(Mo,V)_5C_4T_x$ (n=4). In contrast to all previously known MXenes, the recently discovered $Mo_4VC_4T_x$ solid solution MXene with five M layers shows twinning in the M layers (146). The M sites of MXenes can be occupied by one or more transition metal atoms, forming solid solutions or ordered structures. The ordered double transition metal MXenes exist as in-plane ordered structures $[i\text{-MXenes}, e.g., (Mo_{2/3}Y_{1/3})_2CT_x]$; in-plane vacancy structures (e.g., $W_{2/3}CT_x$); and out-of-plane ordered structures (o-MXenes), where either one layer of M" transition metal is sandwiched between two layers of M' transition metals (e.g., $Mo_2TiC_2T_x$) or two layers of M" transition metals are sandwiched between two layers of M' transition metals (e.g., $Mo_2Ti_2C_3T_x$). Other arrangements, such as one or three layers of M" sandwiched between the layers of M' (bottom row) in the M_5X_4 structure, may be possible. Faded images at the bottom of the figure represent predicted structures such as high-entropy MXenes and higher-order single M or o-MXenes that have yet to be experimentally verified.

However, further investigations are required to provide a better understanding of the arrangement of X site atoms in these MXenes. In bulk carbides and nitrides of transition metals, oxygen can substitute for either C or N in the lattice, forming oxycarbides or oxynitrides, respectively. The possibility of such substitution in MXenes should be investigated.

The surface of MXenes (Fig. 2A) is covered with single or mixed terminations (T = O, OH, NH, F, Cl, Br, S, Se, Te), depending on the synthesis process used and MXene composition (8, 24). These terminations can be altered or completely removed by postprocessing (24, 25), and this has a profound effect on properties.

Synthesis of MXenes in fluorine- and chlorine-containing acidic solutions results in MXenes with mixed surface terminations where the composition of T_x (surface groups) in the MXene formula can be described as $(OH)_mO_xF_yCl_z$ (25–27). Nuclear magnetic resonance (NMR), elastic neutron scattering, x-ray photoelectron spectroscopy (XPS), and scanning transmission electron microscopy (STEM) techniques along with density functional theory (DFT) predictions have suggested a random distribution for F, OH, and O with a varying ratio, depending on the synthesis method, where F and O terminations usually dominate over OH groups in the dry state (26, 28–30). The T

atoms can reside at the surface in different positions relative to M and X atoms. The most energetically favorable and thermodynamically stable site for these moieties is on the surface of M₂C, M₃C₂, and M₄C₃ layers, centered above the transition metal atoms of the atomic plane beneath the outer layer [facecentered cubic (fcc) site] (28, 31). Functional groups can also arrange on the surface in a way that they reside on top of the X atoms (hcp sites). Although there is competition at room temperature between different groups to reside in the preferred thermodynamically stable sites, STEM studies have shown that F atoms are the ones occupying the fcc sites, whereas O atoms can reside at both sites (28). The composition and coordination of MXenes' terminations can be modified through thermal processing and vacuum annealing (28, 32, 33). For example, the surface of $Ti_3C_2T_x$ and Ti_3CNT_x MXenes can be completely defluorinated at temperatures above 550°C (28, 32, 33).

The structure of MXenes produced using aqueous etchants contains two types of intercalated (structural) water, physisorbed and chemisorbed. The physisorbed water can be removed at temperatures below 200°C, while the monolayer of chemisorbed water with hydrogen bonding to the surface may still remain intercalated in the MXene (33, 34), requiring vacuum annealing at temperatures reaching 500°C for removal (25, 34).

Cl-terminated multilayer MXenes ($M_{n+1}X_nCl_2$) can be produced by etching in Lewis acids forming CuCl₂ or CdCl₂ salt melts (24, 35, 36). Bromides, such as CdBr2, can be used instead of CdCl₂ to achieve Br terminations (24). These uniform halogen terminations (specifically Br) at the surface of MXenes can be removed to produce a collapsed 3D structure, where there is substantial interlayer interaction between the MXene sheets, similar to electrides (37). These terminations can also be exchanged with other functional groups through subsequent surface reactions, further expanding the range of MXene compositions. For example, heating of Ti₃C₂Br₂ to 300°C in the presence of LiH removed surface terminations and produced multilayer Ti₃C₂ (24). Similarly, MXenes with Se, Te, S, NH, and O terminations have been produced (24). Rietveld refinement, extended x-ray absorption fine structure (EXAFS), and pair distribution function (PDF) analyses have shown that the structure of MXenes slightly changes depending on the type of uniform surface terminations, resulting in in-plane compressive or tensile strain (24).

Theory and experimental demonstration of MXene properties Electronic properties

The physical and (electro)chemical properties of MXenes are dependent on their composition and structure as well as their surface and

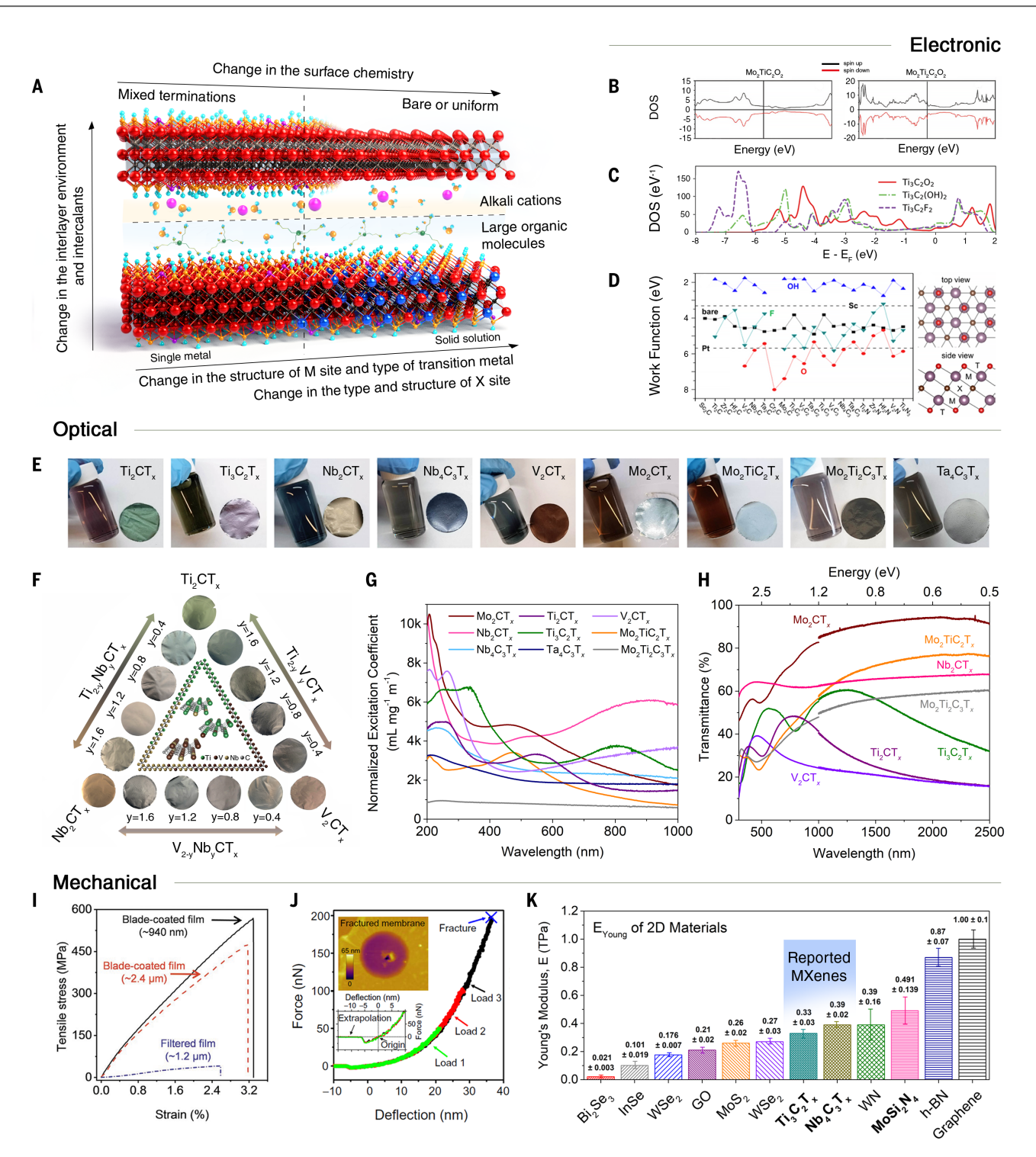


Fig. 2. Electronic, optical, and mechanical properties of MXenes. (**A**) Schematic illustration of different compositional and structural factors determining electronic and optical properties of MXenes. (**B**) Total DOS for $Mo_2TiC_2O_2$ and $Mo_2Ti_2C_3O_2$, showing the effect of MXene structure (40). (**C**) DOS of Ti_3C_2 , $Ti_3C_2O_2$, $Ti_3C_2O_3$, and $Ti_3C_2F_2$, showing the effect of surface chemistry on electronic properties of MXenes (44). (**D**) Dependence of the work function of MXenes on their surface chemistry (45). (**E**) The color of colloidal solutions of various MXenes and their corresponding freestanding films (54). (**F**) Digital photographs of three $M'_{2-y}M''_yCT_x$ solid solution systems, showing the change in optical properties and color of freestanding MXene films due to a gradual change in the stoichiometry (55). (**G**) UV-vis-NIR optical extinction properties

of aqueous dispersions of various 2D transition metal carbides (54). (**H**) UV-vis-NIR transmittance spectra from 300 to 2500 nm for MXene thin films (54). (**I**) Tensile stress versus strain curves of $Ti_3C_2T_x$ films with different thickness produced by vacuum-assisted filtration and blade coating (60). (**J**) Force-deflection curves of a bilayer $Ti_3C_2T_x$ flake at different loads. The lower inset is a detailed view of the same curves showing the center of origin. The top inset shows an AFM image of a punctured flake with no sign of catastrophic rupture (61). (**K**) Comparison of the effective Young's moduli of single-layer $Ti_3C_2T_x$ and $Nb_4C_3T_x$ with other 2D materials tested in similar nano-indentation experiments (62). [(B) to (K) adapted with permission from (40, 44, 45, 54, 55, 60–62)]

interlayer chemistry (Fig. 2A). The electron transport behavior of most MXenes is similar to metals, with resistivity decreasing linearly with temperature $\left(\frac{dR}{dT} > 0\right)$ (38, 39). However, altering the transition metal type and the structure of the M site of MXenes can result in a negative temperature dependence of resistivity $\left(\frac{dR}{dT} < 0\right)$ and, therefore, MXenes with semiconductor-like behavior (32, 40). Examples of the latter include Mo₂CT_x, Nb₂CT_x, and V_2CT_x (21, 41). Moreover, while $Ti_3C_2T_x$ has metallic conductivity, $Mo_2TiC_2T_x$ o-MXene in which the outer Ti layers of Ti₃C₂T_x are substituted with Mo shows semiconductor-like behavior (40). Figure 2B shows an example of a change in the density of states (DOS) of MXenes by changing the M-site structure. Tuning the M site of o-MXenes by varying the outer-layer transition metals (M") has been predicted to enable MXenes with attractive magnetic properties, primarily of antiferromagnetic character (42). Ferromagnetism has been predicted for o-MXenes with Mn in the middle layer and Mn nitrides (42). A magnetic glass transition in Cr₂TiC₂T_x was reported at around 30 to 35 K (43). Theoretical predictions continue to provide guidance for potential structures and compositions. For example, in some simulated o-MXenes, the central M" layers are non-spin-polarized, but the M' lavers at the surface are under octahedral crystal forcefields, resulting in band splitting in their 3d orbitals and, therefore, a net spin moment defining the magnetic order of the o-MXene (42).

All MXenes without surface terminations are predicted to be metallic conductors in which the free electrons of transition metals act as carriers (24, 39). However, surface terminations can change the DOS and shift the Fermi level, making them electronically tunable, unlike conventional metals (Fig. 2C) (44). For some MXenes other than Ti₃C₂T_{xx} bandgap opening and a change from metallic to semiconducting behavior has been predicted, as well as a large variation in their work functions (Fig. 2D) (39, 45). Superconductivity has been observed in Nb_2CT_x ($T_x = Se$, S, or NH), whereas nonterminated or O-terminated multilayer Nb₂C did not show a superconducting transition (24). MXene surface terminations also affect their thermal transport and thermoelectric properties (46). The intercalants, which are often used for delamination, also affect the electronic properties of multilayers and films (32). The intercalation of large organic cations, such as tetrabutylammonium (TBA⁺), between MXene flakes results in a large interlayer spacing (47, 48), which hinders interflake electron hopping, making the produced films less conductive. In contrast, intercalated alkali cations tend to preserve a small interlayer distance and high conductivity of MXenes (49, 50). Deintercalation of water and TBA+ from $Mo_2TiC_2T_x$ and Ti_3CNT_x MXenes resulted in a transition from ensemble semiconducting (a negative dR/dT) to a metallic behavior (32).

The flake size, stoichiometry, surface chemistry, and point defects (mostly vacancies in the M and C sublattices either inherited from the precursor or induced by etching) also affect the physical properties of MXenes and their chemical stability (51). Larger $Ti_3C_2T_x$ flakes with fewer defects show better intraflake electron transport and chemical stability, and their conductivity can reach 20,000 S cm⁻¹ (52).

Optical properties

MXenes show longitudinal and transversal surface plasmon modes in the visible and nearinfrared (vis-NIR) range, where transversal plasmons are shown to be independent of the flake's lateral dimension (38, 53). They also show strong absorption in the ultraviolet (UV) range owing to interband transitions. The optical properties of MXenes are dependent on the type and structure of the M and X sites as well as the stoichiometry of surface terminations. Different MXenes have plasmonic peaks spanning the entire vis-NIR spectrum region (54, 55) and plasmonic colors in transmission (colloidal solution or thin film) and reflection (solid-state multilayer films), as shown in Fig. 2, E and F (38). Generally, by decreasing the nvalue of MXenes, the prominent excitation peaks in their optical spectra shift to higher energies (54). For example, $Ti_3C_2T_x$ MXene has an emerald green color in transmission and a purple color in reflection, with a characteristic absorbance peak centered at 1.6 eV [wavelength (λ) of ~770 nm] (54), whereas V_2CT_n has a greenish blue color in transmission and a brownish gold color in reflection, with no absorption peak in the ultraviolet-vis-NIR (UVvis-NIR) spectrum region (Fig. 2, G and H). The direct current conductivity to optical conductivity figure of merit for transparent Ti₃C₂T_n thin films has been reported to reach a value of 15, which is superior to that of graphene and carbon nanotubes (56), owing to the lower sheet resistance (~201 ohms per square) of $Ti_3C_2T_x$ thin films with optical transmittance of ~87%. V₂CT_x has shown an even higher figure of merit (57). In solid solution MXenes, a change in the M':M" ratio results in different plasmonic colors, as shown in Fig. 2F for several compositions in the (Ti, Nb)₂CT_x and (Ti, $V)_2CT_x$ systems (55). Nonlinear optical behavior (decreasing transmittance with increasing light intensity) was observed for $Ti_3C_2T_x$ thin films, explained by a plasmon-induced increase in the ground-state absorption, which results in a saturable absorption at a wavelength of 1064 nm (58).

Mechanical properties

While the high elastic modulus of MXenes, similar to that of bulk carbides (59), was predicted in the early studies (1), experimental

exploration of mechanical properties of MXenes is just starting. Ti₃C₂T_x MXene films (thickness of ~940 nm) prepared by a blade coating technique have shown a tensile strength of ~560 MPa (Fig. 2I), which exceeds that of aluminum foil (60). In terms of fundamental mechanical properties, so far, only single-layer flakes of $Ti_3C_2T_x$ and $Nb_4C_3T_x$ have been experimentally tested using atomic force microscopy (AFM) nanoindentation (61, 62). Young's modulus (E) of single-layer Ti₃C₂T_x reached 0.33 TPa. Figure 2J shows the force-deflection curve during the AFM nanoindentation experiment on bilayer $Ti_3C_2T_x$ (61). $Ti_3C_2T_x$ membranes did not catastrophically fail, even upon rupture, and the sharp AFM tip only poked a hole (Fig. 2J, inset), demonstrating their high fracture toughness. In addition, the measured modulus of single-layer Nb₄C₃T_x reached ~0.39 TPa (62)—still lower than the theoretically predicted limit, because of the presence of point defects and surface terminations (63). The breaking strength of $Nb_4C_3T_x$ reached 26 ± 1.6 GPa. Figure 2K compares the reported Young's modulus values of various 2D materials (62), including the newly discovered vapor-grown MoSi₂N₄ (64). Nitride-based MXenes are predicted to have a higher in-plane Young's modulus than carbide MXenes (65).

Synthesis and processing

The strong bonding between M and A atoms in the MAX phases and layered carbides does not allow direct mechanical exfoliation of single MX layers from the MAX phases (2), even though intense shearing is known to produce multilayer MAX flakes (66). Therefore, a chemical or electrochemical selective etching approach enabled by the difference in the bonding energy and chemical reactivity of bonds in layered precursors is required (1, 11). The metallic bonding between M- and A-layer atoms in many MAX phases is weaker than the ionic and/or covalent bonding present between M and X atoms (3), and therefore it can be broken using a kinetically and thermodynamically favorable chemical reaction in an etchant capable of dissolving the reaction products. Some preliminary studies suggest that the difference in interlayer bonding is crucial, while others stress the importance of the electrochemical conditions from calculated Pourbaix diagrams (67). The complexity of selective etching will require advancement of the simulation approaches, in line with the recently suggested use of high-throughput computations and machine learning methods (9, 68).

Removal of the A-layer atoms in wet chemical etching techniques and surface functionalization of formed MX layers (Fig. 3A) result in lattice expansion along the c axis, as evident from broadening and downshift of the x-ray diffraction (XRD) peaks corresponding to (00l) planes of MAX phases (2). If etching is

complete and all of the MAX phase is transformed into MXene, the corresponding XRD peaks of the MAX phase lose their intensity and ultimately disappear, being replaced by broad reflections from MXene's basal planes (8, 11). The etching results in exfoliation of 2D MX layers and their spontaneous termination with various surface functional groups, which reduce their chemical potential and increase their thermodynamic stability (8).

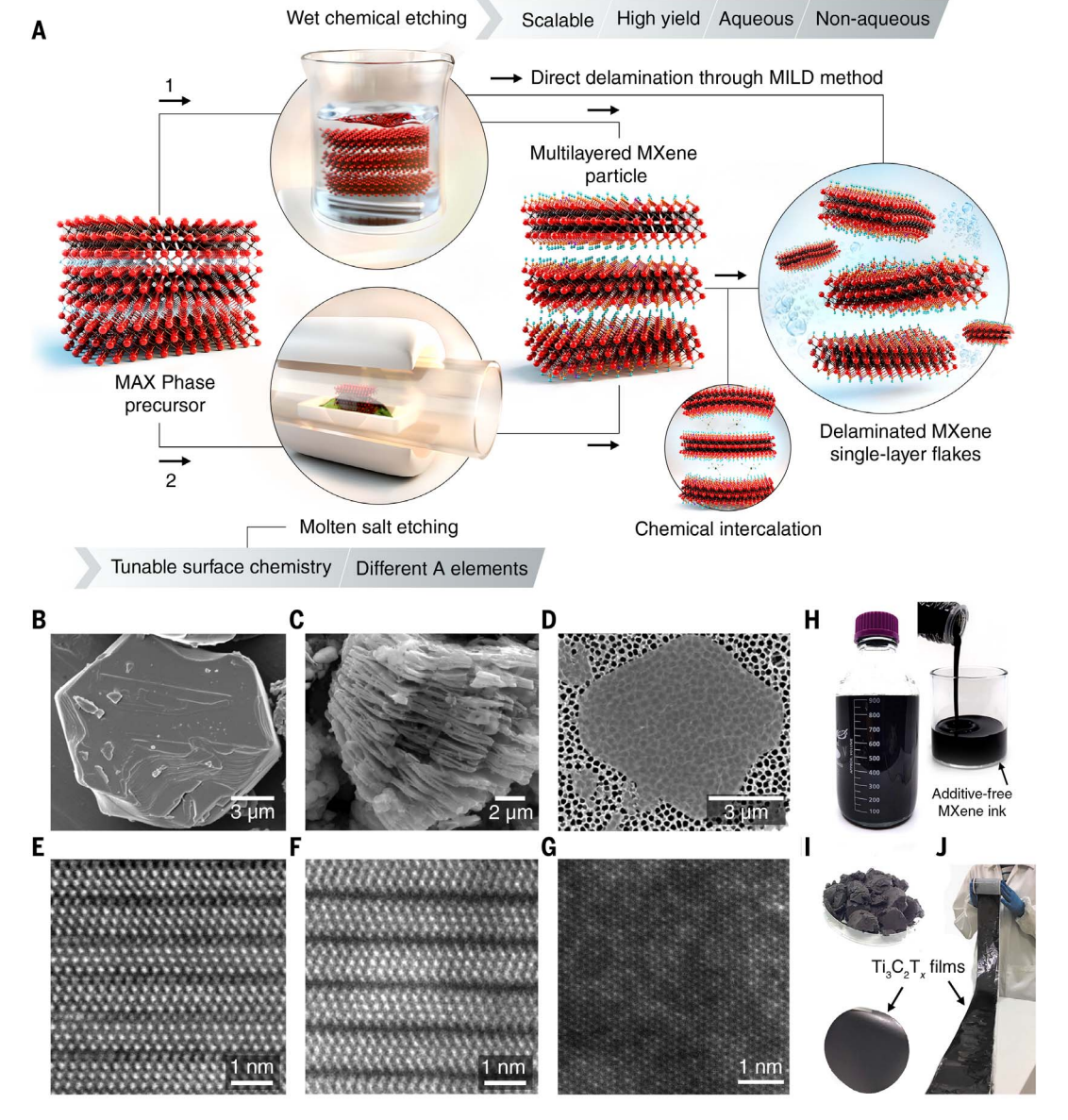
Different concentrations of HF are commonly used to etch Al-containing MAX phases (1, 8, 11). While HF has proven to be a very good etchant for selective removal of Al, it is very corrosive and poses severe health risks, which should be considered during MXene synthesis. Nevertheless, using HF as the etchant usually results in formation of *ml*-MXene particles with a signature accordion-shape mor-

phology, because of the evolution of hydrogen gas during synthesis (note that not seeing this morphology does not necessarily mean that the etching has been unsuccessful). The produced ml-MXenes can be subsequently delaminated into single- or few-layer flakes through chemical intercalation of organic molecules such as dimethyl sulfoxide (DMSO), tetrabutylammonium hydroxide (TBAOH), tetramethylammonium hydroxide (TMAOH), or n-butylamine (47, 48). Because of their anionic surface terminations, d-MXenes produced by wet chemical etching have a zeta potential below -30 mV and form stable colloidal solutions. Figure 3, B to D, shows typical morphologies of a Ti₃AlC₂ MAX phase particle, ml-Ti₃C₂T₂, and d-Ti₃C₂T_x. Figure 3, E to G, shows STEM images of Ti₃AlC₂, ml-Ti₃C₂T_x, and a plane-view of singlelayer d-Ti₃C₂T_x produced from it, respectively.

Etching in fluoride salts (LiF, NaF, KF, etc.) mixed with hydrochloric (HCl) or other acids is another approach that provides a safer pathway for MXene synthesis (5). In this approach, known as the MILD (minimally intensive layer delamination) method, mixing HCl and metal fluoride results in the formation of HF and an intercalant (e.g., Li ions if LiF salt is used), and therefore both etching and intercalation/ delamination can be done simultaneously (69). Also, because of the presence of Li cations in between flakes, the MXene flakes produced by the MILD method show claylike rheological behavior (5, 70). $Ti_3C_2T_x$ produced by this method does not show the accordion-like particle morphology observed in HF-etched *ml*-MXenes. Although the MILD method is applicable to just a few MXenes (15, 41, 69), it provides better control over flake size and quality (71, 72),

Fig. 3. Synthesis and processing of MXenes. (A) Schematic illustration of two approaches to produce MXenes by removal of A layers from MAX phases and related lavered compounds. In the first approach, the MAX phase is selectively etched in fluoride ioncontaining acids. By this method, multilayered MXene particles or in situ delaminated 2D flakes (using the MILD method) can be obtained. In the second approach, the MAX phase is selectively etched in molten salts. The product is usually multilayered MXene particles, which can then be delaminated through intercalation. (B) Scanning electron microscope (SEM) image of a hexagonal-shape Ti₃AlC₂ MAX phase crystal (52). (C) SEM image of a Ti₃C₂T_x MXene particle, derived from Ti₃SiC₂ by selective etching of Si layers in molten salt (36). (D) Topview SEM image of a delaminated $Ti_3C_2T_x$ flake (52). (**E**) STEM image of a M₃AX₂ MAX phase (Ti₃AIC₂) particle. (F) The corresponding STEM image of an mI-M₃X₂T_x MXene particle (Ti₃C₂T_x). (G) Atomically resolved plane-view STEM image of single-layer Ti₃C₂T_y (28). (H to J) Digital photographs of $\sim 1 L$ of delaminated $Ti_3C_2T_x$

solution (166), highly concentrated $T_{i3}C_2T_x$ ink (167), multilayered $T_{i3}C_2T_x$ MXene particles (166), a $T_{i3}C_2T_x$ film prepared by vacuum-assisted filtration of a colloidal MXene solution (168), and large-area, mechanically robust $T_{i3}C_2T_x$ film produced by blade coating (60). [(E) and (F) courtesy of



P. O. Å. Persson; (B) to (D) and (G) to (J) adapted with permission from (14, 28, 36, 52, 60, 166, 167)]

producing $Ti_3C_2T_x$ flakes with lateral dimensions of up to 15 μ m and no pinholes (71). Etching in HF or HCl solution produces ml- $Ti_3C_2T_x$ (52, 73), which can be delaminated with LiCl instead of organic intercalants (52), resulting in higher delamination yields of ~60%. Water-free synthesis of Ti₃C₂T_x MXene in ammonium dihydrogen fluoride (NH4HF2) dissolved in polar organic solvents (e.g., propylene carbonate) produces $Ti_3C_2T_x$ with a very large interlayer spacing of 21 to 51 Å (depending on the solvent), which was attributed to cointercalation of NH₄⁺ cation complexes with solvent molecules (74). Generally, water-free etchants promote chemical stability of MXene and minimize its oxidation, while elimination of fluoride-containing etchants is expected to substantially reduce the defects on MXenes and enable tunable terminations. Examples of these can be seen in two recently developed etching approaches, one using halogen compounds, i.e., tetrabutyl ammonium bromide (75) in anhydrous cyclohexane to synthesize Ti₃C₂Br₂ from Ti₃AlC₂, and another using iodine in anhydrous acetonitrile (CH3CN) to prepare $Ti_3C_2T_x$ with oxygen terminations (76).

Wet chemical etching techniques have produced MXenes from Al-containing MAX phases and related ceramics (non-MAX phases), with a few exceptions where Ga double-layers (77), $[Al(Si)]_4C_4$ (78) and Al_3C_3 (79) carbide layers, or Si monolayers (80) were removed using HF or a mixture of HF and oxidants, such as H₂O₂. Molten salts that form Lewis acids (CuCl₂, CdCl₂, or CdBr₂) can selectively etch a larger variety of A-layer elements (Al. Zn. Si. Ga. etc.) from MAX phases at moderate temperatures (24, 35, 36). In this approach (Fig. 3A), the A element (i.e., Si in Ti₃SiC₂) is oxidized (in this case, to Si⁴⁺) by the cation (Cu²⁺) forming a volatile compound (SiCl₄ boils at 57.6°C) that is readily removed, vielding a Cl- or Br-terminated MXene (e.g., Ti₃C₂Cl₂) as the result of charge compensation by the anions (24, 36). Because the M-Cl or M-Br bonds on the surface of MXenes have a lower bond energy compared to M-F or M-O terminations, they can be modified or removed (24). For example, Ti₃C₂Br₂ was transformed to Ti₃C₂Te₂ and Ti₃C₂S₂ by reaction with Li2Te and Li2S, respectively, in a CsBr/ KBr/LiBr eutectic melt (24). Rapid synthesis of Ti₃C₂T_x (in milliseconds) through application of a megahertz frequency acoustic excitation to the Ti₃AlC₂ MAX phase in LiF solution (81) is the latest effort toward costeffective preparation of MXenes, Yet, among different developed etching techniques, the wet chemical etching of MAX phases in fluoridecontaining acidic solutions results in the highest yield of MXene products and therefore remains the method of choice for largescale manufacturing.

MXenes can be processed into various shapes and morphologies, as shown for $Ti_3C_2T_x$ in

Fig. 3, H to J. The liquid crystalline MXene dispersions in water can be processed into fibers (82) or freestanding films using vacuum-assisted filtration or blade coating methods (60, 69), and printed into patterns with different geometries without any additives (83). Spin, dip, and spray coating techniques as well as layer-by-layer assembly, screen printing, inkjet printing, and other methods have been used to deposit MXenes onto various substrates (80, 84-87).

Optical and electronic applications

Low sheet resistance and good transparency [0.1 to 8 kilohms per square at ~40 to 90% transmittance in the visible range (88)1 make $Ti_3C_2T_x$ thin films promising for optoelectronic applications where flexible transparent conductive electrodes (TCEs) are required, such as solar cells, liquid crystal displays (LCDs), and organic light-emitting diodes (OLEDs). Ti₃C₂T_x TCEs with ~4-nm thickness and transmittance of 91% have been used in transparent solidstate supercapacitors (56), delivering excellent volumetric capacitance. Reversible intercalation of protons or organic ions (e.g., TMAOH) into transparent Ti₃C₂T_x films results in a reversible change in their color, enabling electrochromic devices (89).

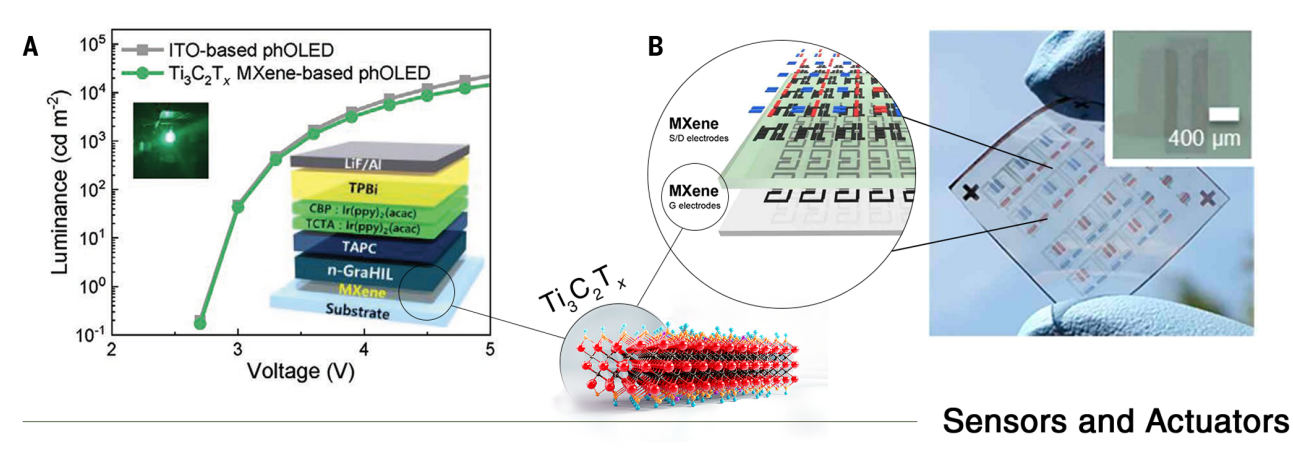
The work function of MXenes can also be tuned through modulation of their bulk and surface. For example, the $Ti_3C_2T_x$ MXene has been predicted to have work functions ranging from ~1.81 to ~6.15 eV for completely OH- or O-terminated surface chemistries, respectively (45). The high conductivity and tunable work function promise a low energy barrier for hole injection, and this MXene has been used as TCEs in OLEDs (90) and photonic diodes (58). An OLED containing a $Ti_3C_2T_x$ TCE (device structure is shown in the inset of Fig. 4A) with a work function tuned to 5.1 eV had external quantum efficiency of ~28.5% (90), comparable with state-of-the-art commercial OLEDs. $Ti_3C_2T_x$ has been used in photovoltaics to tune the work function and electrode contact interfaces for an improved charge extraction process (91). For example, $Ti_3C_2T_x$ MXene was incorporated in several components of a perovskite solar cell with a TiO2 electron transport layer, where the $Ti_3C_2T_x$ MXene-modified perovskite solar cell showed ~5% higher power conversion efficiency (PCE) than the original cell (91). MXenes with modulated work functions have also been used as electrodes in fieldeffect and thin-film transistors (FET and TFT) and logic circuits (92, 93). Figure 4B shows a large array of organic FETs fabricated entirely with $Ti_3C_2T_x$ electrodes.

Gas sensors based on MXenes can detect volatile organic compounds (VOCs) and non-polar gases, such as ammonia, ethanol, and acetone, at room temperature, mostly because of their metallic core channels and surface

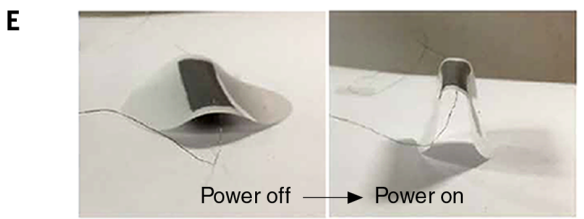
functional groups that result in strong adsorption energies for these gas molecules (94, 95). A gas sensor based on Ti₃C₂T_x delivered a two orders of magnitude greater signal-to-noise ratio and an experiential limit of detection for VOCs lower than other gas sensors based on 2D materials at room temperature (94). MXenes have also been used in biosensors (96, 97), strain sensors (98), actuators, and soft robotics (99-101). Strain sensors based on Ti₃C₂T_x-PVA (polyvinyl alcohol) hydrogels exhibited stretching of more than 3400% (Fig. 4C) and an instantaneous self-healing property with the capability of detecting complex hand gestures owing to the 3D structure of a network of MXene flakes inside the hydrogel matrix (Fig. 4D) (98). A Ti₃C₂T_x-cellulose composite soft actuator on a polycarbonate membrane showed a fast response and low-power actuation deforming up to a maximum bending angle of 147° at 5.1 V (Fig. 4E) (101). Electrochemical activity in various analytes, hydrophilicity, and rich surface chemistry make MXenes attractive for biosensing (Fig. 4F shows a MXene device schematic for biomolecule sensing). Freestanding MXene membranes have been used as solid-state nanopore platforms for rapid detection and translocation of single molecules (96).

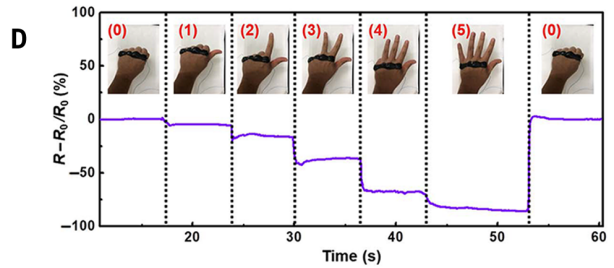
High metallic conductivity and abundant free electrons are important for electromagnetic interference (EMI) shielding. Ti₃C₂T_x films of 1- to 2-um thickness showed an EMI shielding effectiveness (EMI SE) of ~50 dB (99.999% protection), and 92 dB at a thickness of 45 um (102). Various MXene compositions have been investigated for EMI shielding applications, demonstrating the role of the structure and composition of MXene in their EMI shielding properties (103). Figure 4G shows the EMI SE_{Total} of various MXenes and conventional materials versus their thickness (104). A 40-µm-thick Ti₃CNT_x MXene film with an electronic conductivity of ~1800 S cm⁻¹, which is about one-fifth that of Ti₃C₂T_x and orders of magnitude lower than that of copper, showed an EMI SE_{Total} of 116 dB (104). Although the interaction of free electrons with incident electromagnetic waves is believed to dominate their reflection, the anomalous performance of Ti₃CNT_x films can be attributed to their layered, metamaterial-like structure (104). The fundamental reason behind this anomaly still needs to be understood. High conductivity and solution processability of Ti₃C₂T_x has also attracted attention for microwave absorbance and terahertz shielding (72), as well as wireless communication, antennas, and radio frequency identification (RFID) tags delivering comparable performances to copper antennas at a small fraction of their weight and thickness (73, 105). For example, Ti₃C₂T_x MXene patch antennas with a thickness of 5.5 µm have shown a radiation

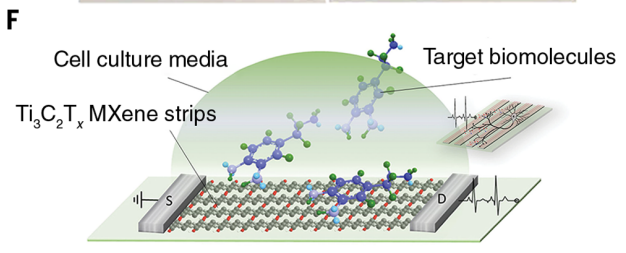
Optoelectronics



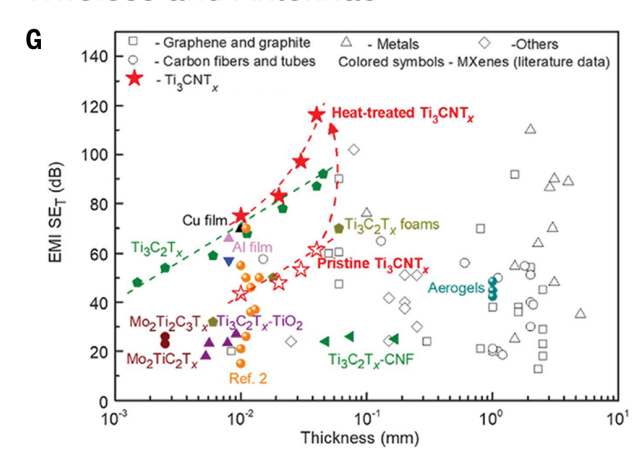








Wireless and Antennas



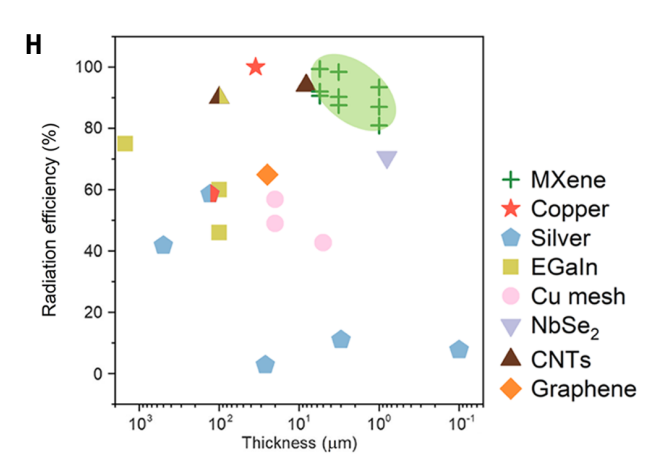


Fig. 4. Applications of MXenes in optoelectronics, sensors and actuators, electromagnetic interference shielding, and wireless communication and antennas. (A) Luminance of light-emitting diodes (LEDs) with indium tin oxide (ITO) and MXene transparent electrodes at different voltages. Left inset shows an optical image of a MXene-based green phosphorescent organic LED (phOLED), and the right inset shows a schematic of this device (90). (B) Photograph and device schematic of a large-scale electrode array for organic field effect transistors (OFETs) using $Ti_3C_2T_x$ (92). (C) Photograph demonstrating the stretchability of MXene hydrogel (98). (D) Resistance change of a MXene hydrogel strain sensor in response to different hand gestures (98). (E) Response

of a $Ti_3C_2T_x$ –cellulose soft actuator on a polycarbonate substrate to the applied voltage (101). (**F**) Illustration of a MXene FET with $Ti_3C_2T_x$ electrodes for biomolecular sensing (169). (**G**) Comparison of EMI shielding efficiencies (SE_T) of Ti_3CNT_x , $Ti_3C_2T_x$, $Mo_2TiC_2T_x$, and $Mo_2Ti_2C_3T_x$ films with carbons and metals (104). At comparable thicknesses, the performance of annealed Ti_3CNT_x surpasses that of all other materials. (**H**) A comparison of radiation efficiency versus thickness for MXene patch antennas with those made of metals, carbons, and other materials (105). EGaIn, eutectic gallium-indium; CNTs, carbon nanotubes. [(A) to (H) adapted with permission from (90, 92, 98, 101, 104, 105, 169)]

efficiency of ~99% and a return loss value of $-49\,$ dB at a frequency of 16.4 GHz (105). Figure 4H compares radiation efficiency of ${\rm Ti}_3{\rm C}_2{\rm T}_x$ wireless antennas with that of other materials.

Energy storage, harvesting, and electrocatalysis

The use of MXenes for electrochemical energy storage (Li-ion batteries and supercapacitors) was an early area of interest (4, 106), and we refer readers to reviews on the subject for details (8, 107). Figure 5A highlights properties of MXenes that govern their electrochemical behavior. Transition metal core layers in MXenes facilitate rapid electron transport through the electrode enabling charge storage at ultra-high rates, and a transition metal oxide-like surface provides redox-active sites for pseudocapacitive charge storage. The combination of these two properties renders MXenes promising electrode materials for ultrafast supercapacitors and batteries. In addition, subnanometer interlayer slits between 2D sheets allow rapid ion intercalation and transport, and they can be expanded through pre-intercalation, pillaring, and making hybrids or heterostructures with other 2D materials or carbon nanotubes to fit ions of different sizes (50, 85, 108, 109). The surface terminations of MXenes can be tailored toward certain redox chemistries. For example, Ti₃C₂I₂ recently showed reversible high-voltage I^o/I⁺ redox behavior in a zinc-iodide battery (110). The electrochemical intercalation of cations with different sizes and charges from both aqueous and nonaqueous electrolytes has been observed for a variety of MXenes (4, 6, 7, 50, 111, 112). MXenes have been tested in various kinds of energy storage devices, including metal-ion, metal-sulfur, and metaloxygen batteries. However, these materials usually have shown sloping charge-discharge profiles without a distinct plateau, typical for conventional Li- and Na-ion batteries. In Li-S (Na-S/K-S) batteries, MXenes show strong adsorption of polysulfides, high conductivity, and catalytic ability. They can also be used as a barrier for polysulfide transport on the separator, current collector, and Li host, preventing the growth of dendrites (113-115). Moreover, integrating MXenes into heterostructures with other 2D materials or hybrid architectures with high-capacity conversiontype battery materials enables battery electrodes with higher capacities, high-rate capabilities, and long cycle life. MXenes not only improve charge and ion transport inside the electrode but also can accommodate large volume expansion of the high-capacity components acting as conductive binders (109, 116, 117).

In supercapacitors, $Ti_3C_2T_x$ electrodes deliver a volumetric and gravimetric capacitance of up to ~1500 F cm⁻³ and ~400 F g⁻¹, respectively, in protic H_2SO_4 electrolyte, and thin-

film electrodes maintain more than half of their initial capacitance at 10-ms chargedischarge (118) (Fig. 5B). This shows that redox processes can be used for storage and delivery of energy at extremely high rates, as long as electronic and ionic conductivity of electrodes is sufficient. Similarly, d-Mo_{4/3}CT_x i-MXene freestanding paper electrode has shown a low charge transport resistivity combined with a volumetric capacitance of 1100 F cm⁻³ at 10 mV s⁻¹, which was increased to ~1600 F cm⁻³ (~700 F g⁻¹) through post-annealing in argon (18). These results are substantially higher than for Mo₂CT_x MXene, indicating a beneficial effect of MXene vacancies on the electrochemical energy storage. In organic electrolytes. the charge storage in $Ti_3C_2T_x$ MXene depends not only on the kind of cation but also on the solvent (119). This solvent-selective behavior is shown in Fig. 5C, where replacing the acetonitrile solvent with propylene carbonate doubled the Li⁺ storage capacity of Ti₃C₂T_r electrode through complete desolvation of inserted Li ions (119). Consequently, proper pairing of MXene with electrolytes is required.

As solution-processable 2D materials, MXenes can enable flexible, on-chip, printable, and wearable energy storage and harvesting devices (83, 120). $\text{Ti}_3\text{C}_2\text{T}_x$ MXene-based microsupercapacitors prepared on different substrates, including paper, were capable of filtering high frequency ripples in AC (alternating current) line (121). Figure 5D shows a wafer-scale array of a MXene microsupercapacitor fabricated for AC-line filtering applications (121). $\text{Ti}_3\text{C}_2\text{T}_{x^-}$ coated conductive yarns and energy storing textiles with good environmental stability and washability have been demonstrated and used to fabricate knitted device with interdigitated electrodes (Fig. 5E).

MXenes have been used for energy harvesting and conversion applications, such as flexible triboelectric nanogenerators that can harvest energy from human motion (122, 123). The high light-to-heat conversion efficiency of $Ti_3C_2T_x$ has rendered it one of the best materials for solar-driven water steam generation (124). Ultrasound energy harvesting has also been demonstrated (125). Moreover, lamellar freestanding $Ti_3C_2T_x$ membranes with confined ion-selective nanofluidic channels were shown to be capable of osmotic energy harvesting under a salinity gradient (126, 127).

The oxygen atom terminations on the surface of MXenes can effectively act as the catalytic active sites for hydrogen evolution reaction (HER) (128, 129). Therefore, controlling their surface stoichiometry toward lower fluorine and higher oxygen concentrations lowers the overpotential for HER in MXenes (130). Mobased MXenes, which have few or no fluorine terminations, show better HER performance compared with $\text{Ti}_3\text{C}_2\text{T}_x$ or Ti_2CT_x (128, 130). Introduction of ordered vacancies, as in i-

MXenes, improves the performance even further, as demonstrated for $Mo_{4/3}CT_x$ and $W_{4/3}CT_x$ (131). Whereas in transition metal dichalcogenides (TMDs), only edges are catalytically active, the entire basal plane of MXene participates in catalysis, providing a high current density (129). The possibility of creating vacancies on M sites enables these materials to support single-atom precious metal catalysts, as demonstrated for platinum atoms immobilized on Mo-vacancies on the Mo₂TiC₂T_x surface (132). The produced catalyst showed ~40 times higher catalytical mass activity than commercially available Pt-on-carbon catalysts. MXenes have also been explored for catalyzing the oxygen evolution reaction (OER) (133) and No. reduction reactions (NRR) (134).

Biomedical and environmental applications

Biocompatibility and low cytotoxicity of most MXene compositions, such as $Ti_3C_2T_x$ (135), Nb_2CT_r (136), and $Ta_4C_3T_r$ (137), as well as their plasmon resonance and high photothermal conversion efficiency in the near-IR and IR range (124) make these materials promising for cancer theranostics (Fig. 5F). $Ta_4C_3T_x$ has attracted particular attention because of its higher photothermal efficiency (~44.7%) compared with $Ti_3C_2T_x$ (137). Soybean phospholipidmodified $Ta_4C_3T_x$ nanosheets were used for in vitro and in vivo photothermal ablation of breast cancer cells (137), where >90% of the MXene-incubated cells were killed upon application of a NIR laser (Fig. 5G). MXenes have also been used for drug delivery (138) and magnetic resonance imaging (MRI)-guided tumor hyperthermia applications (136).

MXenes have higher resistance to biofouling and accumulation of microorganisms and bacteria compared with graphene oxide (139) and therefore have been targeted as filtration and desalination membranes and as implantable devices. $Ti_3C_2T_x$ was used in implantable brain electrodes with superior impedance and in vivo neural recording performance in comparison with gold microelectrodes (Fig. 5H) (140). Similar performance has been shown by MXene electrode arrays for high-density, highresolution surface electromyography, where they outperformed noble metals and allowed gel-free application (141). Inspired by its exciting electro-optical properties, a Ti₃C₂T_x TCE on acrylate was explored in intraocular lenses mimicking the accommodative function of the eye's natural lens (142). Figure 5H illustrates an example of an adjustable-focus lens based on spin-coated Ti₃C₂T_x electrodes and a liquid crystal with the capability to change its refractive index (under an electric field) resulting in an optical power and change of

The ability of $Ti_3C_2T_x$ and $Mo_2TiC_2T_x$ MXenes to remove urea from dialysate by adsorption is more efficient than other sorbents (143, 144)

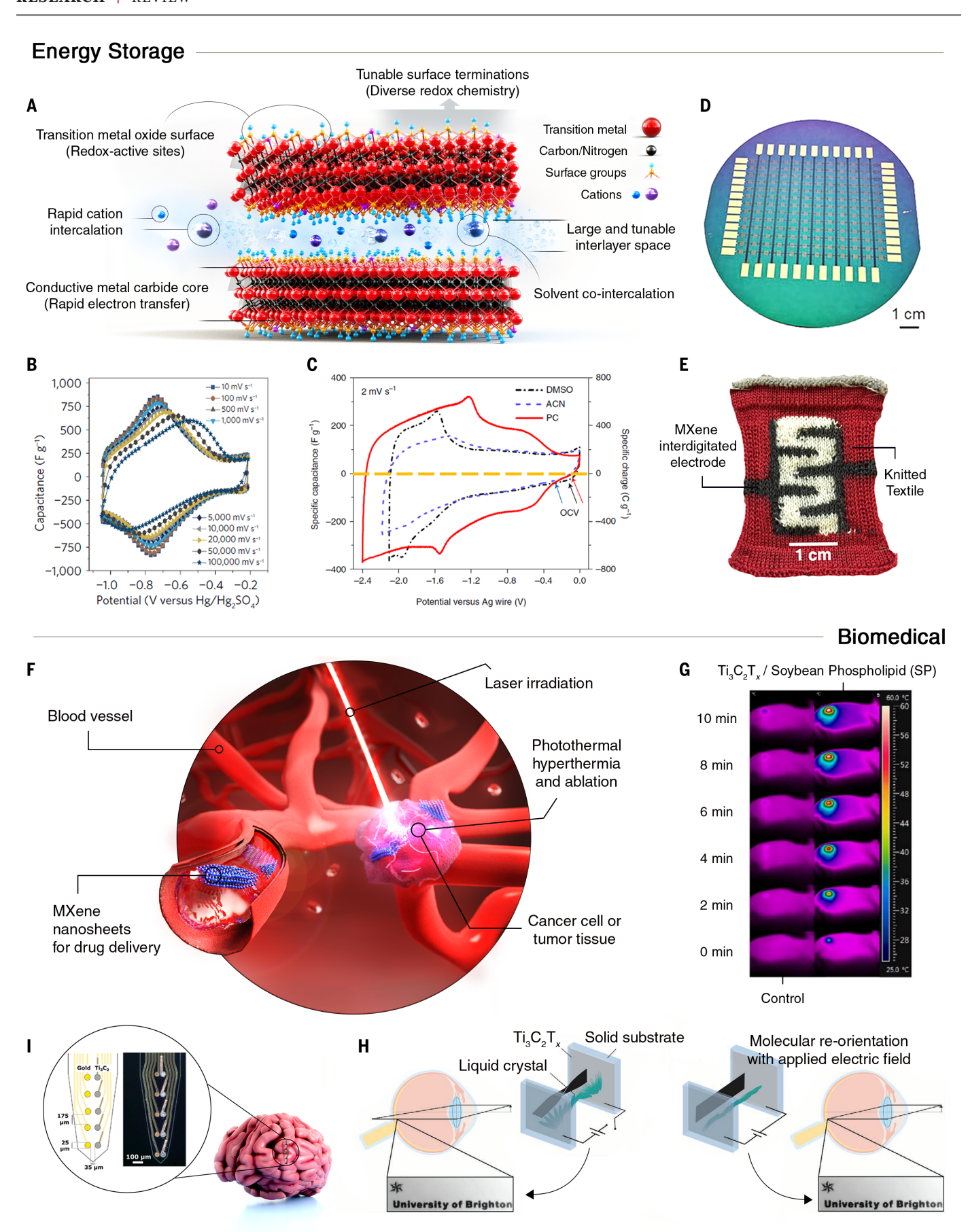


Fig. 5. Energy storage and biomedical applications of MXenes. (**A**) Schematic illustration showing MXenes' electrochemical properties for ion storage applications. (**B**) Cyclic voltammetry (CV) data collected at scan rates from 10 to $100,000 \text{ mV} \cdot \text{s}^{-1}$ for a 90-nm-thick $\text{Ti}_3\text{C}_2\text{T}_x$ film (118). (**C**) Influence of an electrolyte's solvent on the lithium-ion storage capacity of $\text{Ti}_3\text{C}_2\text{T}_x$: CV curves of microporous $\text{Ti}_3\text{C}_2\text{T}_x$ electrode in 1 M lithium bis(trifluoromethanesulfonyl)imide (LiTFSI) in DMSO, acetonitrile (ACN), or propylene carbonate (PC) electrolytes (119). (**D**) A digital photograph showing the wafer scale fabrication of an array of 143 MXene microsupercapacitors (121). (**E**) Photograph of a knitted textile with an interdigitated pattern made using $\text{Ti}_3\text{C}_2\text{T}_x$ MXene-coated cotton yarn to produce electrodes for wearable textile supercapacitor

(170). (**F**) Schematic illustration of biomedical applications of MXenes. (**G**) Infrared thermal images of a mouse with a 4T1 tumor before and after intravenous injection of 20 mg/kg dose of $Ti_3C_2T_x$ -soybean phospholipid under 808-nm laser irradiation (1.5 W cm⁻²) at different time intervals (171). (**H**) Schematics and bright-field microscopy image of an electrode array made from $Ti_3C_2T_x$ /Au for brain neural activity recording (140). (**I**) An adjustable-focus lens constructed with glass slides coated with $Ti_3C_2T_x$ and sandwiching a liquid crystal (LC) layer in twisted nematic orientation. Molecular reorientation of the LC layer upon application of an electric field allows focusing of the lens (142). [(D), (E), and (G) to (I) adapted with permission from (118, 119, 121, 140, 142, 170, 171)]

and may enable development of a wearable dialysis system known as an artificial kidney. The high adsorption efficiency for urea and uric toxins arises from narrow slits between functionalized and charged MXene sheets, which act as adsorption sites.

MXenes and beyond: Discovery and design of related 2D structures

Synthesis of *i*-MXenes, including structures with ordered vacancies; demonstration of Ti_4C_3 , Ti_5C_4 (145), and $Mo_4VC_4T_x$ MXenes (146); chemical vapor deposition (CVD) growth of nanometersthin Mo_2C (147); synthesis of numerous solid solution MXenes; transformation of carbide MXenes into nitrides by high-temperature treatment in ammonia (148); and topochemical transformation of TMDs into 2D W_5N_6 and Mo_5N_6 nitrides (149) suggest the possibility of synthesis of many more 2D carbides and nitrides, which should be guided by high-throughput simulations (68) and machine learning (9) for accelerated material discovery.

Other related 2D structures with different chemical formulas, such as 2D MC2 carbides (e.g., TiC₂—pending experimental verification) (150), vapor-grown 2D $MoSi_2N_4$ (64), ultrathin MAX phases (MAXenes) (66), and the emerging family of 2D borides (MBenes) with a similar formula to MXenes but with boron-occupied X sites (151, 152) have been predicted, and in some cases their partially exfoliated particles have been produced or ultrathin crystals grown. Carbide and nitride electrides, such as Ca_2N (37), which have low environmental stability but attractive physical properties, are also of interest. For example, vapor-grown 2D MoSi₂N₄ has a Young's modulus of ~0.5 TPa and a breaking strength of ~66 GPa (64). DFT calculations have predicted a large family of semiconducting 2D structures with a general formula of MA₂Z₄, where M is a transition metal, A is Si or Ge, and Z can be N, P, or As (64). Other calculations have predicted 2D MC2 carbides (e.g., NbC₂, TaC₂, and MoC₂) for HER and OER (153), and partially etched borides have shown promise for electrocatalytic HER applications (151, 152). Similar to MAX phases, the M-A bonds in MAB phases are weaker than M-B bonds (154), potentially allowing selective etching of A-elements. However, previous efforts only resulted in multilayer MBenes where periodic removal of Al layers forms stacking faults containing a single Al layer (only one of the Al double layers was removed during the etching from the structure of MoAlB), creating stacking sequences (i.e., Mo_2AlB_2) that hinder further Al deintercalation and exfoliation (151). Therefore, more research is required to identify the approriate precursors and achieve complete exfoliation of MAB phases to MBenes.

Precursors are of critical importance for MXene synthesis in general. On one hand, it is important to achieve their low-cost synthesis from ores and coal, coke, or carbon black by an Acheson-like process or self-propagating high-temperature synthesis. MXenes containing Earth-abundant elements such as Ti and carbon or nitrogen are of practical interest for large-volume applications, such as energy storage or water purification and desalination, and availability of low-cost precursors will be an enabling factor. On the other hand, synthesis of new MAX phases designed as precursors for specific MXenes is equally important. as further expansion of the family will not be possible otherwise. For example, W-containing MXene became possible because of the synthesis of W-based i-MAX, as W-based traditional MAX phases are not stable. M5C4 MXene was enabled by adding a second M element. Computation-driven design of MAX phases and other precursors for MXene synthesis may assist in expansion of the family and adding new compositions and structures.

Figure 6 illustrates the potential directions for future discovery and design of 2D metal carbides, nitrides, and borides, as well as property tuning pathways that can open the possibility to move beyond the state-of-the-art and toward predicted extreme properties. Several studies have suggested tunable magnetism and ferromagnetic properties of nitride MXenes (155), which would enable MXene-based spintronic devices. In-plane chemically ordered i-MXenes such as those potentially originating from rare Earth (RE)-based Mo_{4/3}RE_{2/3}AlC i-MAX are attractive, as the magnetic elements are located at the apexes of a 2D triangular lattice, which is an arrangement that may result in a wide range of magnetic phenomena and intricate ordered (collinear, chiral, etc.) or disordered (spin ice or liquid, etc.) ground states. Similarly, some oxygen-terminated MXenes (Mo- and Cr-containing M2CO2 MXenes or Mo₂TiC₂O₂ and Mo₂Ti₂O₃ o-MXenes) have been predicted to be topological insulators when tailored with certain bandgaps (156, 157). The molten salt technique allows synthesis of fully oxygen-terminated MXenes and therefore may lead to experimental verification of the predicted topological insulators. Also, computationally guided synthesis and structural design approaches should be utilized to investigate the possibility of producing superconducting MXenes and enabling their use in magnetic imaging, quantum interfaces, and other applications.

Outlook

Over the past 10 years, the world of 2D transition metal carbides and nitrides expanded with the synthesis of M5C4Tx, i-MXenes (with or without divacancies in their basal planes), o-MXenes, and numerous solid solutions. Control over their physical, mechanical, and electrochemical properties via atomistic design has been demonstrated, even though ~50 MXenes reported so far constitute a small part of the family. Composition-dependent optical properties have been shown for solid solution MXenes. Reversible tuning of work function, plasmon resonance, and Fermi level by surface chemistry have been demonstrated for several MXenes. A combination of their elastic properties and mechanical strength, exceeding that of other solution-processed 2D materials, with high metallic conductivity and diverse plasmonic properties can be useful in multifunctional nanocomposites. MXenes have shown redox charge storage and delivery within milliseconds, detection of trace amounts of various gases with ultrahigh sensitivity, and the ability to adsorb urea and shield against microwave radiation. However, for predicting which MXenes will show the best radiation-shielding performance, interactions of individual nanometerthin layers with electromagnetic waves and the related quantum effects should be considered, as continuum electrodynamics does not explain unmatched EMI shielding properties of titanium-based MXenes.

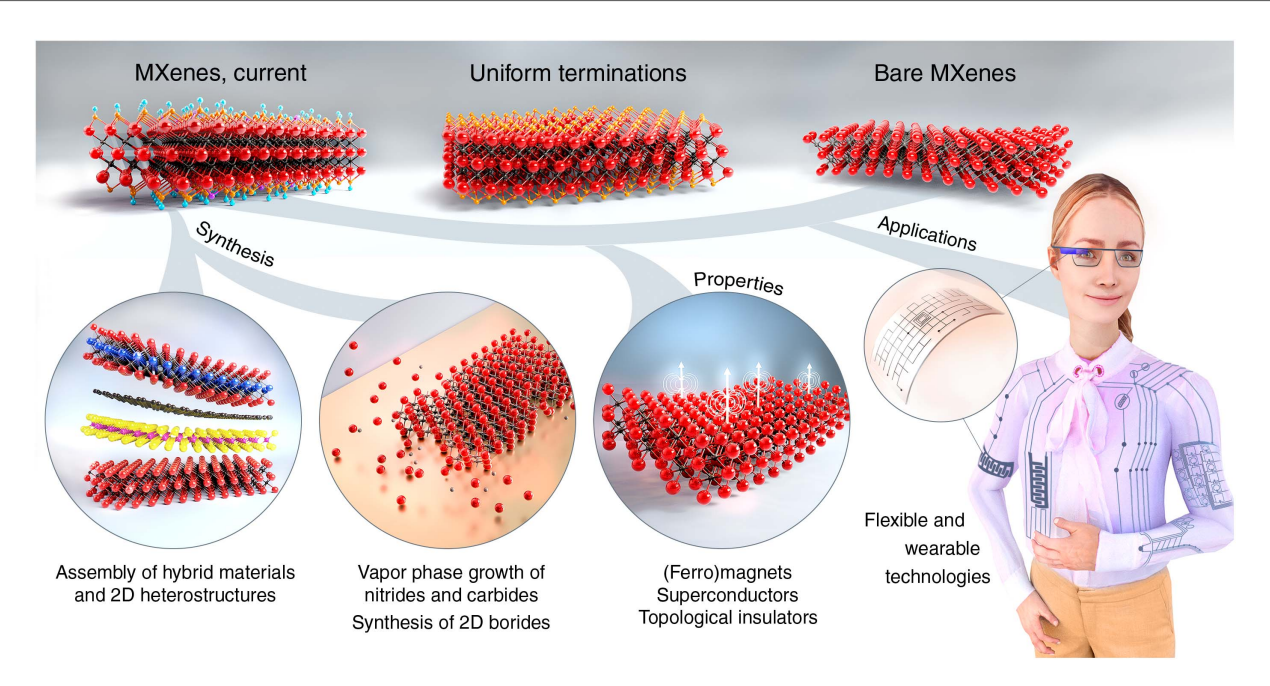


Fig. 6. Synthesis and structural design of MXenes. The discovery of new MXene structures and compositions, and precise control of their surface terminations, as well as their combination with other 2D materials into superlattices and 2D heterostructures, will enable emergence of new properties and expand the use of MXenes in various fields, including flexible and wearable devices for energy storage and harvesting, sensors, actuators, optical lenses, artificial memory devices, quantum computing, and Internet of Things (IoT) devices. [The base 3D model for the female character was obtained from and courtesy of renderpeople.com]

The use of molten salt or halogen-containing organic solvent etchants enabled synthesis of MXenes with Cl or Br terminations with the possibility to exchange them with other moieties through postprocessing. These redoxactive terminated surfaces make MXenes useful in a variety of energy systems including supercapacitors and batteries, showing promise as active materials in anodes and cathodes, binders, current collectors, and electrocatalysts. Understanding the charge storage mechanisms in different MXenes, mechanisms of suppression of metal dendrite growth, dynamics of intercalation of multivalent cations (Mg²⁺, Ca²⁺, or Al³⁺) into MXenes, and building high-power, high-energy all-MXene energy storage devices are all attractive goals.

Because of their compositional and structural variety and tailorable properties, MXenes are now being studied in many fields, beyond what we have covered in this Review. Outstanding mechanical properties, low friction coefficient, high conductivity with the electrochemically tunable Fermi level, and optical properties make them attractive for soft robotics and actuators (101), lasers and photonics (49, 158, 159), water desalination and environmental remediation (160), (multi)functional lightweight metal-matrix (161) and ceramicmatrix composites (162), memory devices and bioinformatics (163–165), tribology, and other applications.

There are still many challenges that must be addressed to unleash the full potential of MXenes. Efficient, scalable, and cost-effective

etching techniques and delamination routes need to be developed for MXenes beyond Ti₃C₂T_x. i-MXenes, o-MXenes, and solid solution MXenes, including high-entropy ones, are of great interest owing to a wide range of possibilities in tuning their structures and properties. Nitride MXenes have been predicted to have a variety of attractive properties, from ferromagnetism to higher conductivity than carbides or semiconducting properties (155). However, only a few nitrides have been madenone of them magnetic, despite availability of their parent MAX phases. Some o-MXenes are expected to be topological insulators. Tunable superconductivity, large Seebeck coefficient in semiconducting MXenes, work functions ranging from 2 to 8 eV, mechanism of electron/ charge transport in-plane and out-of-plane of MXenes, role of interlayer chemistry on interflake conduction of MXene films, electrochemical tuning of their optoelectronic behavior, and other attractive properties are to be explored. Etching routes with higher selectivity toward M-A bonds than M-N bonds should be developed to exfoliate nitride MAX phases. Beyond currently known MXenes, other 2D carbide and nitride structures, including vapor-grown 2D nitrides (MA₂Z₄), computationally predicted MC2 carbides, and 2D borides are important targets.

It is important to mention that MXenes complement properties of other 2D materials, and they can be seen as building blocks that add metallically conductive, plasmonic, electrochemical, or catalytical properties to hybrid

materials and structures and when combined with graphene, boron nitride, dichalcogenides, and other 2D materials. This opens a path to building hybrid and heterostructure materials and devices with programmed properties using additive manufacturing and self-assembly from solution.

Methods and protocols should be established to improve the chemical stability of MXenes, especially for applications as singlelayer flakes and thin films. Better understanding of the role of precursor structure and stoichiometry, as well as the etchant composition and postprocessing treatments on synthesis and properties of resulting MXenes will facilitate scale-up and large-volume manufacturing of MXenes at the commercial scale. Synthesis of MXenes from non-Al based MAX phases or MAX phase analogs must be further explored. CVD and physical vapor deposition synthesis of 2D MXenes can open the door to preparing high-quality (defect-free), large singlelayer crystals, and bare MXenes, which can facilitate study of fundamental physical (quantum) properties and electronic applications of these materials in areas such as bioelectronics and electrochemical artificial synapses or neuromorphic computing.

REFERENCES AND NOTES

- M. Naguib et al., Two-dimensional nanocrystals produced by exfoliation of Ti₃AlC₂ Adv. Mater. 23, 4248–4253 (2011). doi: 10.1002/adma.201102306; pmid: 21861270
- M. Naguib et al., Two-dimensional transition metal carbides. ACS Nano 6, 1322–1331 (2012). doi: 10.1021/nn204153h; pmid: 22279971

- M. Sokol, V. Natu, S. Kota, M. W. Barsoum, On the chemical diversity of the MAX phases. *Trends Chem.* 1, 210–223 (2019). doi: 10.1016/j.trechm.2019.02.016
- M. R. Lukatskaya et al., Cation intercalation and high volumetric capacitance of two-dimensional titanium carbide. Science 341, 1502–1505 (2013). doi: 10.1126/ science.1241488; pmid: 24072919
- M. Ghidiu, M. R. Lukatskaya, M. Q. Zhao, Y. Gogotsi, M. W. Barsoum, Conductive two-dimensional titanium carbide 'clay' with high volumetric capacitance. *Nature* 516, 78–81 (2014). doi: 10.1038/nature13970; pmid: 25470044
- M. Naguib et al., New two-dimensional niobium and vanadium carbides as promising materials for Li-ion batteries. J. Am. Chem. Soc. 135, 15966–15969 (2013). doi: 10.1021/ ia405735d; pmid: 24144164
- X. Wang et al., Pseudocapacitance of MXene nanosheets for high-power sodium-ion hybrid capacitors. Nat. Commun. 6, 6544 (2015). doi: 10.1038/ncomms7544; pmid: 25832913
- B. Anasori, M. R. Lukatskaya, Y. Gogotsi, 2D metal carbides and nitrides (MXenes) for energy storage. *Nat. Rev. Mater.* 2, 16098 (2017). doi: 10.1038/natrevmats.2016.98
- N. C. Frey et al., Prediction of synthesis of 2D metal carbides and nitrides (MXenes) and their precursors with positive and unlabeled machine learning. ACS Nano 13, 3031–3041 (2019). doi: 10.1021/acsnano.8b08014; pmid: 30830760
- B. Anasori, Y. Gogotsi, Eds., 2D Metal Carbides and Nitrides (MXenes): Structure, Properties and Applications (Springer International Publishing, 2019).
- M. Naguib, V. N. Mochalin, M. W. Barsoum, Y. Gogotsi, 25th anniversary article: MXenes: a new family of two-dimensional materials. Adv. Mater. 26, 992–1005 (2014). doi: 10.1002/ adma.201304138; pmid: 24357390
- W. Hong, B. C. Wyatt, S. K. Nemani, B. Anasori, Double transition-metal MXenes: Atomistic design of twodimensional carbides and nitrides. MRS Bull. 45, 850–861 (2020). doi: 10.1557/mrs.2020.251
- R. Meshkian et al., Theoretical stability and materials synthesis of a chemically ordered MAX phase, Mo₂ScAlC₂, and its two-dimensional derivate Mo₂ScC₂ MXene. Acta Mater. 125, 476–480 (2017). doi: 10.1016/j. actamat 2016.12.008
- B. Anasori et al., Two-dimensional, ordered, double transition metals carbides (MXenes). ACS Nano 9, 9507–9516 (2015). doi: 10.1021/acsnano.5b03591; pmid: 26208121
- M. Dahlqvist et al., Prediction and synthesis of a family of atomic laminate phases with Kagomé-like and in-plane chemical ordering. Sci. Adv. 3, e1700642 (2017). doi: 10.1126/sciadv.1700642; pmid: 28776034
- Q. Tao et al., Two-dimensional Mo_{1.33}C MXene with divacancy ordering prepared from parent 3D laminate with in-plane chemical ordering. Nat. Commun. 8, 14949 (2017). doi: 10.1038/ncomms14949; pmid: 28440271
- A. Mockute et al., Materials synthesis, neutron powder diffraction, and first-principles calculations of (Mo_xSc_{1x})₂AlC i-MAX phase used as parent material for MXene derivation. Phys. Rev. Mater. 3, 113607 (2019). doi: 10.1103/ PhysRevMaterials.3.113607
- B. Ahmed, A. El Ghazaly, J. Rosen, i-MXenes for energy storage and catalysis. Adv. Funct. Mater. 30, 2000894 (2020). doi: 10.1002/adfm.202000894
- R. Meshkian et al., W-based atomic laminates and their 2D derivative W_{1,3}C MXene with vacancy ordering. Adv. Mater. 30, e1706409 (2018). doi: 10.1002/adma.201706409; pmid: 29633399
- I. Persson et al., Tailoring structure, composition, and energy storage properties of MXenes from selective etching of inplane, chemically ordered MAX phases. Small 14, e1703676 (2018). doi: 10.1002/smll.201703676; pmid: 29611285
- P. Urbankowski et al., Synthesis of two-dimensional titanium nitride Ti₄N₃ (MXene). Nanoscale 8, 11385–11391 (2016). doi: 10.1039/C6NR02253G; pmid: 27211286
- B. Soundiraraju, B. K. George, Two-dimensional titanium nitride (Ti₂N) MXene: Synthesis, characterization, and potential application as surface-enhanced Raman scattering substrate. ACS Nano 11, 8892–8900 (2017). doi: 10.1021/ acsnano.7b03129; pmid: 28846394
- A. Djire et al., Pseudocapacitive storage in nanolayered Ti₂NT_x MXene using Mg-ion electrolyte. ACS Appl. Nano Mater. 2, 2785–2795 (2019). doi: 10.1021/acsanm.9b00289
- V. Kamysbayev et al., Covalent surface modifications and superconductivity of two-dimensional metal carbide MXenes. Science 369, 979–983 (2020). doi: 10.1126/science.aba8311; pmid: 32616671

- M. Seredych et al., High-temperature behavior and surface chemistry of carbide MXenes studied by thermal analysis. Chem. Mater. 31, 3324–3332 (2019). doi: 10.1021/acs. chemmater.9b00397
- M. A. Hope et al., NMR reveals the surface functionalisation of Ti₃C₂ MXene. Phys. Chem. Chem. Phys. 18, 5099–5102 (2016). doi: 10.1039/C6CP00330C; pmid: 26818187
- X. Wang et al., Atomic-scale recognition of surface structure and intercalation mechanism of Ti₃C₂X. J. Am. Chem. Soc. 137, 2715–2721 (2015). doi: 10.1021/ja512820k; pmid: 25688582
- I. Persson et al., On the organization and thermal behavior of functional groups on Ti₃C₂ MXene surfaces in vacuum. 2D Mater. 5, 015002 (2018). doi: 10.1088/2053·1583/aa89cd
- K. J. Harris, M. Bugnet, M. Naguib, M. W. Barsoum, G. R. Goward, Direct measurement of surface termination groups and their connectivity in the 2D MXene V₂CT_x using NMR spectroscopy. *J. Phys. Chem. C* 119, 13713–13720 (2015). doi: 10.1021/acs.jpcc.5b03038
- H. W. Wang, M. Naguib, K. Page, D. J. Wesolowski, Y. Gogotsi, Resolving the structure of Ti₃C₂T_x MXenes through multilevel structural modeling of the atomic pair distribution function. Chem. Mater. 28, 349–359 (2016). doi: 10.1021/acs. chemmater.5b04250
- T. Schultz et al., Surface termination dependent work function and electronic properties of Ti₃C₂T_x MXene. Chem. Mater. 31, 6590–6597 (2019). doi: 10.1021/acs.chemmater.9b00414
- J. L. Hart et al., Control of MXenes' electronic properties through termination and intercalation. Nat. Commun. 10, 522 (2019). doi: 10.1038/s41467-018-08169-8; pmid: 30705273
- I. Persson et al., How much oxygen can a MXene surface take before it breaks? Adv. Funct. Mater. 30, 1909005 (2020). doi: 10.1002/adfm.201909005
- R. Thakur et al., Insights into the thermal and chemical stability of multilayered V₂CT_x MXene. Nanoscale 11, 10716–10726 (2019). doi: 10.1039/C9NR03020D; pmid: 31120085
- M. Li et al., Element replacement approach by reaction with Lewis acidic molten salts to synthesize nanolaminated MAX phases and MXenes. J. Am. Chem. Soc. 141, 4730–4737 (2019). doi: 10.1021/jacs.9b00574; pmid: 30821963
- Y. Li et al., A general Lewis acidic etching route for preparing MXenes with enhanced electrochemical performance in non-aqueous electrolyte. Nat. Mater. 19, 894–899 (2020). doi: 10.1038/s41563-020-0657-0; pmid: 32284597
- D. L. Druffel et al., Experimental demonstration of an electride as a 2D material. J. Am. Chem. Soc. 138, 16089–16094 (2016). doi: 10.1021/jacs.6b10114; pmid: 27960319
- K. Hantanasirisakul, Y. Gogotsi, Electronic and optical properties of 2D transition metal carbides and nitrides (MXenes). Adv. Mater. 30, e1804779 (2018). doi: 10.1002/ adma.201804779; pmid: 30450752
- M. Khazaei, A. Ranjbar, M. Arai, T. Sasaki, S. Yunoki, Electronic properties and applications of MXenes: A theoretical review. J. Mater. Chem. C 5, 2488–2503 (2017). doi: 10.1039/C7TC00140A
- B. Anasori et al., Control of electronic properties of 2D carbides (MXenes) by manipulating their transition metal layers. Nanoscale Horiz. 1, 227–234 (2016). doi: 10.1039/ CSNH00125K; pmid: 32260625
- J. Halim et al., Synthesis and characterization of 2D molybdenum carbide (MXene). Adv. Funct. Mater. 26, 3118–3127 (2016). doi: 10.1002/adfm.201505328
- W. Sun, Y. Xie, P. R. C. Kent, Double transition metal MXenes with wide band gaps and novel magnetic properties. *Nanoscale* 10, 11962–11968 (2018). doi: 10.1039/ C8NR00513C; pmid: 29904773
- K. Hantanasirisakul et al., Evidence of a magnetic transition in atomically thin Cr₂TiC₂T_x MXene. Nanoscale Horiz. 5, 1557–1565 (2020). doi: 10.1039/D0NH00343C; pmid: 33089267
- N. M. Caffrey, Effect of mixed surface terminations on the structural and electrochemical properties of two-dimensional Ti₃C₂T₂ and V₂CT₂ MXenes multilayers. Nanoscale 10, 13520–13530 (2018). doi: 10.1039/C8NR03221A; pmid: 29972202
- Y. Liu, H. Xiao, W. A. Goddard 3rd, Schottky-barrier-free contacts with two-dimensional semiconductors by surfaceengineered MXenes. J. Am. Chem. Soc. 138, 15853–15856 (2016). doi: 10.1021/jacs.6b10834; pmid: 27960324
- M. Khazaei, M. Arai, T. Sasaki, M. Estili, Y. Sakka, Twodimensional molybdenum carbides: Potential

- thermoelectric materials of the MXene family. *Phys. Chem. Chem. Phys.* **16**, 7841–7849 (2014). doi: 10.1039/C4CP00467A; pmid: 24643873
- M. Naguib, R. R. Unocic, B. L. Armstrong, J. Nanda, Large-scale delamination of multi-layers transition metal carbides and carbonitrides "MXenes". *Dalton Trans.* 44, 9353–9358 (2015). doi: 10.1039/C5DT01247C; pmid: 25912071
- O. Mashtalir et al., Intercalation and delamination of layered carbides and carbonitrides. Nat. Commun. 4, 1716 (2013). doi: 10.1038/ncomms2664; pmid: 23591883
- L. Wu et al., MXene-based nonlinear optical information converter for all-optical modulator and switcher. Laser Photonics Rev. 12, 1800215 (2018). doi: 10.1002/ lonr.201800215
- A. VahidMohammadi, M. Mojtabavi, N. M. Caffrey, M. Wanunu, M. Beidaghi, Assembling 2D MXenes into highly stable pseudocapacitive electrodes with high power and energy densities. Adv. Mater. 31, 1806931 (2019). doi: 10.1002/adma.201806931
- K. Maleski, C. E. Ren, M. Q. Zhao, B. Anasori, Y. Gogotsi, Size-dependent physical and electrochemical properties of two-dimensional MXene flakes. ACS Appl. Mater. Interfaces 10, 24491–24498 (2018). doi: 10.1021/acsami.8b04662; pmid: 29956920
- T. S. Mathis et al., Modified MAX phase synthesis for environmentally stable and highly conductive Ti₃C₂ MXene. ACS Nano 15, 6420–6429 (2021). doi: 10.1021/ acsnano.0c08357; pmid: 33848136
- J. K. El-Demellawi, S. Lopatin, J. Yin, O. F. Mohammed, H. N. Alshareef, Tunable multipolar surface plasmons in 2D Ti₃C₂T_x MXene flakes. ACS Nano 12, 8485–8493 (2018). doi: 10.1021/acsnano.8b04029; pmid: 30020767
- K. Maleski, C. E. Shuck, A. T. Fafarman, Y. Gogotsi, The broad chromatic range of two-dimensional transition metal carbides. Adv. Opt. Mater. 9, 2001563 (2020). doi: 10.1002/ adom.202001563
- M. Han et al., Tailoring electronic and optical properties of MXenes through forming solid solutions. J. Am. Chem. Soc. 142, 19110–19118 (2020). doi: 10.1021/jacs.0c07395; pmid: 33108178
- C. J. Zhang et al., Transparent, flexible, and conductive 2D titanium carbide (MXene) films with high volumetric capacitance. Adv. Mater. 29, 1702678 (2017). doi: 10.1002/adma.201702678; pmid: 28741695
- G. Ying, S. Kota, A. D. Dillon, A. T. Fafarman, M. W. Barsoum, Conductive transparent V₂CT_x (MXene) films. *FlatChem* 8, 25–30 (2018). doi: 10.1016/j.flatc.2018.03.001
- Y. Dong et al., Saturable absorption in 2D Ti₃C₂ MXene thin films for passive photonic diodes. Adv. Mater. 30, 1705714 (2018). doi: 10.1002/adma.201705714
- Y. G. Gogotsi, R. A. Andrievski, Materials Science of Carbides, Nitrides and Borides (Springer, 1999).
- J. Zhang et al., Scalable manufacturing of free-standing, strong Ti₂C₂T_x MXene films with outstanding conductivity. Adv. Mater. 32, 2001093 (2020). doi: 10.1002/ adma.202001093
- A. Lipatov et al., Elastic properties of 2D Ti₃C₂T_x MXene monolayers and bilayers. Sci. Adv. 4, eaat0491 (2018). doi: 10.1126/sciadv.aat0491; pmid: 29922719
- A. Lipatov et al., Electrical and elastic properties of individual single-layer Nb₄C₃T_x MXene flakes. Adv. Electron. Mater. 6, 1901382 (2020). doi: 10.1002/aelm.201901382
- G. Plummer, B. Anasori, Y. Gogotsi, G. J. Tucker, Nanoindentation of monolayer Ti_{n+1}C_nT_x MXenes via atomistic simulations: The role of composition and defects on strength. Comput. Mater. Sci. 157, 168–174 (2019). doi: 10.1016/ i.commatsci.2018.10.033
- Y.-L. Hong et al., Chemical vapor deposition of layered twodimensional MoSi₂N₄ materials. Science 369, 670–674 (2020). doi: 10.1126/science.abb7023; pmid: 32764066
- N. Zhang, Y. Hong, S. Yazdanparast, M. A. Zaeem, Superior structural, elastic and electronic properties of 2D titanium nitride MXenes over carbide MXenes: A comprehensive first principles study. 2D Mater. 5, 045004 (2018). doi: 10.1088/ 2053-1583/aacfb3
- K. V. Mahesh, R. Rashada, M. Kiran, A. Peer Mohamed, S. Ananthakumar, Shear induced micromechanical synthesis of Ti₃SiC₂ MAXene nanosheets for functional applications. RSC Advances 5, 51242–51247 (2015). doi: 10.1039/ C5RA07756G
- C. Zhan, W. Sun, Y. Xie, D. E. Jiang, P. R. C. Kent, Computational discovery and design of MXenes for energy

- applications: Status, successes, and opportunities. ACS Appl. Mater. Interfaces 11, 24885–24905 (2019). doi: 10.1021/acsami.9b00439; pmid: 31082189
- T. L. Tan, H. M. Jin, M. B. Sullivan, B. Anasori, Y. Gogotsi, High-throughput survey of ordering configurations in MXene alloys across compositions and temperatures. ACS Nano 11, 4407–4418 (2017). doi: 10.1021/acsnano.6b08227; pmid: 28297600
- M. Alhabeb et al., Guidelines for synthesis and processing of two-dimensional titanium carbide (Ti₃C₂T_x MXene). Chem. Mater. 29, 7633–7644 (2017). doi: 10.1021/ acs.chemmater.7b02847
- B. Akuzum et al., Rheological characteristics of 2D titanium carbide (MXene) dispersions: A guide for processing MXenes. ACS Nano 12, 2685–2694 (2018). doi: 10.1021/ acsnano.7b08889; pmid: 29463080
- A. Lipatov et al., Effect of synthesis on quality, electronic properties and environmental stability of individual monolayer Ti₃C₂ MXene flakes. Adv. Electron. Mater. 2, 1600255 (2016). doi: 10.1002/aelm.201600255
- G. Choi et al., Enhanced terahertz shielding of MXenes with nano-metamaterials. Adv. Opt. Mater. 6, 1701076 (2018). doi: 10.1002/adom.201701076
- A. Sarycheva et al., 2D titanium carbide (MXene) for wireless communication. Sci. Adv. 4, eaau0920 (2018). doi: 10.1126/ sciadv.aau0920; pmid: 30255151
- V. Natu et al., 2D Ti₃C₂T₂ MXene synthesized by water-free etching of Ti₃AlC₂ in polar organic solvents. Chem 6, 616–630 (2020). doi: 10.1016/j.chempr.2020.01.019
- A. Jawaid et al., Halogen etch of Ti₃AlC₂ MAX phase for MXene fabrication. ACS Nano 15, 2771–2777 (2021). doi: 10.1021/acsnano.0c08630; pmid: 33502839
- H. Shi et al., Ambient-stable two-dimensional titanium carbide (MXene) enabled by iodine etching. Angew. Chem. Int. Ed. 60, 8689–8693 (2021). doi: 10.1002/ anie.202015627; pmid: 33484049
- R. Meshkian et al., Synthesis of two-dimensional molybdenum carbide, Mo₂C, from the gallium based atomic laminate Mo₂Ga₂C. Scr. Mater. 108, 147–150 (2015). doi: 10.1016/j.scriptamat.2015.07.003
- J. Zhou et al., Synthesis and electrochemical properties of two-dimensional hafnium carbide. ACS Nano 11, 3841–3850 (2017). doi: 10.1021/acsnano.7b00030; pmid: 28375599
- J. Zhou et al., A two-dimensional zirconium carbide by selective etching of Al₃C₃ from nanolaminated Zr₃Al₃C₅. Angew. Chem. Int. Ed. 55, 5008–5013 (2016). doi: 10.1002/ ange.201510432; pmid: 26959082
- M. Alhabeb et al., Selective etching of silicon from Ti₃SiC₂ (MAX) to obtain 2D titanium carbide (MXene). Angew. Chem. Int. Ed. 57, 5444–5448 (2018). doi: 10.1002/ anie.201802232; pmid: 29518271
- A. E. Ghazaly et al., Ultrafast, one-step, salt-solution-based acoustic synthesis of Ti₃C₂ MXene. ACS Nano 15, 4287–4293 (2021). pmid: 33635629
- J. Zhang et al., Additive-free MXene liquid crystals and fibers. ACS Cent. Sci. 6, 254–265 (2020). doi: 10.1021/ acscentsci.9b01217; pmid: 32123744
- C. J. Zhang et al., Additive-free MXene inks and direct printing of micro-supercapacitors. Nat. Commun. 10, 1795 (2019). doi: 10.1038/s41467-019-09398-1; pmid: 30996224
- H. Huang et al., Scalable, and low-cost treating-cuttingcoating manufacture platform for MXene-based on-chip micro-supercapacitors. Nano Energy 69, 104431 (2020). doi: 10.1016/j.nanoen.2019.104431
- W. Tian et al., Layer-by-layer self-assembly of pillared twodimensional multilayers. Nat. Commun. 10, 2558 (2019). doi: 10.1038/s41467-019-10631-0; pmid: 31186411
- H. An et al., Surface-agnostic highly stretchable and bendable conductive MXene multilayers. Sci. Adv. 4, eaaq0118 (2018). doi: 10.1126/sciadv.aaq0118; pmid: 29536044
- M. Mojtabavi et al., Wafer-scale lateral self-assembly of mosaic Ti₃C₂T_x MXene monolayer films. ACS Nano 15, 625–636 (2021). doi: 10.1021/acsnano.0c06393; pmid: 33405898
- K. Hantanasirisakul et al., Fabrication of Ti₃C₂T_x MXene transparent thin films with tunable optoelectronic properties. Adv. Electron. Mater. 2, 1600050 (2016). doi: 10.1002/ aelm.201600050
- K. Hantanasirisakul et al., Effects of synthesis and processing on optoelectronic properties of titanium carbonitride MXene. Chem. Mater. 31, 2941–2951 (2019). doi: 10.1021/ acs.chemmater.9b00401
- 90. S. Ahn et al., A 2D titanium carbide MXene flexible electrode for high-efficiency light-emitting diodes. Adv. Mater.

- **32**, e2000919 (2020). doi: 10.1002/adma.202000919; pmid: 32350958
- A. Agresti et al., Titanium-carbide MXenes for work function and interface engineering in perovskite solar cells. Nat. Mater. 18, 1228–1234 (2019). doi: 10.1038/s41563-019-0478-1; pmid: 31501556
- B. Lyu et al., Large-area MXene electrode array for flexible electronics. ACS Nano 13, 11392–11400 (2019). doi: 10.1021/ acsnano.9b04731; pmid: 31553884
- Z. Wang, H. Kim, H. N. Alshareef, Oxide thin-film electronics using all-MXene electrical contacts. *Adv. Mater.* 30, e1706656 (2018). doi: 10.1002/adma.201706656; pmid: 29473236
- S. J. Kim et al., Metallic Ti₃C₂T_x mxene gas sensors with ultrahigh signal-to-noise ratio. ACS Nano 12, 986–993 (2018). doi: 10.1021/acsnano.7b07460; pmid: 29368519
- E. Lee et al., Room temperature gas sensing of twodimensional titanium carbide (MXene). ACS Appl. Mater. Interfaces 9, 37184–37190 (2017). doi: 10.1021/ acsami.7b11055; pmid: 28953355
- M. Mojtabavi, A. VahidMohammadi, W. Liang, M. Beidaghi, M. Wanunu, Single-molecule sensing using nanopores in twodimensional transition metal carbide (MXene) membranes. ACS Nano 13, 3042–3053 (2019). doi: 10.1021/ acsnano.8b08017; pmid: 30844249
- L. Wu et al., 2D transition metal carbide MXene as a robust biosensing platform for enzyme immobilization and ultrasensitive detection of phenol. Biosens. Bioelectron. 107, 69–75 (2018). doi: 10.1016/j.bios.2018.02.021; pmid: 29448223
- Y. Z. Zhang et al., MXenes stretch hydrogel sensor performance to new limits. Sci. Adv. 4, eaat0098 (2018). doi: 10.1126/sciadv.aat0098; pmid: 29922718
- S. Umrao et al., MXene artificial muscles based on ionically cross-linked Ti₃C₂T_x electrode for kinetic soft robotics. Sci. Robot. 4, eaaw7797 (2019). doi: 10.1126/ scirobotics.aaw7797; pmid: 33137782
- D. Pang et al., Electrochemical actuators based on twodimensional Ti₃C₂T_x (MXene). Nano Lett. 19, 7443–7448 (2019). doi: 10.1021/acs.nanolett.9b03147; pmid: 31536705
- G. Cai, J. H. Ciou, Y. Liu, Y. Jiang, P. S. Lee, Leaf-inspired multiresponsive MXene-based actuator for programmable smart devices. Sci. Adv. 5, eaaw7956 (2019). doi: 10.1126/ sciadv.aaw7956; pmid: 31309158
- F. Shahzad et al., Electromagnetic interference shielding with 2D transition metal carbides (MXenes). Science 353, 1137–1140 (2016). doi: 10.1126/science.aag2421; pmid: 27609888
- 103. M. Han et al., Beyond Ti₃C₂T_x: MXenes for electromagnetic interference shielding. ACS Nano 14, 5008–5016 (2020). doi: 10.1021/acsnano.0c01312; pmid: 32163265
- A. Iqbal et al., Anomalous absorption of electromagnetic waves by 2D transition metal carbonitride Ti₃CNT_x (MXene). Science 369, 446–450 (2020). doi: 10.1126/science.aba7977; pmid: 32703878
- M. Han et al., Solution-processed Ti₃C₂T_x MXene antennas for radio-frequency communication. Adv. Mater. 33, 2003225 (2021). doi: 10.1002/adma.202003225
- M. Naguib et al., MXene: A promising transition metal carbide anode for lithium-ion batteries. Electrochem. Commun. 16, 61–64 (2012). doi: 10.1016/j.elecom.2012.01.002
- M. Okubo, A. Sugahara, S. Kajiyama, A. Yamada, MXene as a charge storage host. *Acc. Chem. Res.* 51, 591–599 (2018). doi: 10.1021/acs.accounts.7b00481; pmid: 29469564
- M. Q. Zhao et al., Flexible MXene/carbon nanotube composite paper with high volumetric capacitance. Adv. Mater. 27, 339–345 (2015). doi: 10.1002/adma.201404140; pmid: 25405330
- 109. C. Chen et al., MoS₂-on-MXene heterostructures as highly reversible anode materials for lithium-ion batteries. Angew. Chem. Int. Ed. 57, 1846–1850 (2018). doi: 10.1002/ anie.201710616; pmid: 29292844
- X. Li et al., Activating the I⁰/I⁺ redox couple in an aqueous I₂–Zn battery to achieve a high voltage plateau. Energy Environ. Sci. 14, 407–413 (2020). doi: 10.1039/D0EE03086D
- III. A. VahidMohammadi, A. Hadjikhani, S. Shahbazmohamadi, M. Beidaghi, Two-dimensional vanadium carbide (MXene) as a high-capacity cathode material for rechargeable aluminum batteries. ACS Nano 11, 11135–11144 (2017). doi: 10.1021/ acsnano.7b05350; pmid: 29039915
- S. Zhao et al., Li-ion uptake and increase in interlayer spacing of Nb₄C₃ MXene. Energy Storage Mater. 8, 42–48 (2017). doi: 10.1016/j.ensm.2017.03.012
- J. Song et al., Immobilizing polysulfides with MXenefunctionalized separators for stable lithium-sulfur batteries. ACS Appl. Mater. Interfaces 8, 29427–29433 (2016). doi: 10.1021/acsami.6b099027: pmid: 27723285

- X. Liang, A. Garsuch, L. F. Nazar, Sulfur cathodes based on conductive MXene nanosheets for high-performance lithium-sulfur batteries. *Angew. Chem. Int. Ed.* 54, 3907–3911 (2015). doi: 10.1002/anie.201410174; pmid: 25650042
- 115. X. Liang, Y. Rangom, C. Y. Kwok, Q. Pang, L. F. Nazar, Interwoven MXene nanosheet/carbon-nanotube composites as Li-S cathode hosts. Adv. Mater. 29, 1603040 (2017). doi: 10.1002/adma.201603040; pmid: 27859697
- 116. X. Guo et al., Boosting sodium storage in two-dimensional phosphorene/Ti₃C₂T_x Mknen annoarchitectures with stable fluorinated interphase. ACS Nano 14, 3651–3659 (2020). doi: 10.1021/acsnano.0c00177; pmid: 32150388
- C. J. Zhang et al., High capacity silicon anodes enabled by MXene viscous aqueous ink. Nat. Commun. 10, 849 (2019). doi: 10.1038/s41467-019-08383-y; pmid: 30787274
- M. R. Lukatskaya et al., Ultra-high-rate pseudocapacitive energy storage in two-dimensional transition metal carbides. Nat. Energy 2, 17105 (2017). doi: 10.1038/ nenergy.2017.105
- X. Wang et al., Influences from solvents on charge storage in titanium carbide MXenes. Nat. Energy 4, 241–248 (2019). doi: 10.1038/s41560-019-0339-9
- Y.-Y. Peng et al., All-MXene (2D titanium carbide) solid-state microsupercapacitors for on-chip energy storage. Energy Environ. Sci. 9, 2847–2854 (2016). doi: 10.1039/C6EE01717G
- Q. Jiang et al., On-chip MXene microsupercapacitors for AC-line filtering applications. Adv. Energy Mater. 9, 1901061 (2019). doi: 10.1002/aenm.201901061
- 122. Y. Dong et al., Metallic MXenes: A new family of materials for flexible triboelectric nanogenerators. Nano Energy 44, 103–110 (2018). doi: 10.1016/j.nanoen.2017.11.044
- 123. M. Salauddin et al., A novel MXene/ecoflex nanocomposite-coated fabric as a highly negative and stable friction layer for high-output triboelectric nanogenerators. Adv. Energy Mater. 11, 2002832 (2021). doi: 10.1002/aenm.202002832
- 124. R. Li, L. Zhang, L. Shi, P. Wang, MXene Ti₃C₂: An effective 2D light-to-heat conversion material. ACS Nano 11, 3752–3759 (2017). doi: 10.1021/acsnano.6b08415; pmid: 28339184
- 125. K. H. Lee et al., Ultrasound-driven two-dimensional Ti₃C₂T_x MXene hydrogel generator. ACS Nano 14, 3199–3207 (2020). doi: 10.1021/acsnano.9b08462; pmid: 32078295
- 126. L. Ding et al., Oppositely charged Ti₃C₂T_x MXene membranes with 2D nanofluidic channels for osmotic energy harvesting. Angew. Chem. 132, 8798–8804 (2020). doi: 10.1002/ange.201915993
- Z. Zhang et al., Mechanically strong MXene/Kevlar nanofiber composite membranes as high-performance nanofluidic osmotic power generators. Nat. Commun. 10, 2920 (2019). doi: 10.1038/s41467-019-10885-8; pmid: 31266937
- 128. Z. W. Seh et al., Two-dimensional molybdenum carbide (MXene) as an efficient electrocatalyst for hydrogen evolution. ACS Energy Lett. 1, 589–594 (2016). doi: 10.1021/acsenergylett.6b00247
- G. Gao, A. P. O'Mullane, A. Du, 2D MXenes: A new family of promising catalysts for the hydrogen evolution reaction. ACS Catal. 7, 494–500 (2017). doi: 10.1021/acscatal.6b02754
- A. D. Handoko et al., Tuning the basal plane functionalization of two-dimensional metal carbides (MXenes) to control hydrogen evolution activity. ACS Appl. Energy Mater. 1, 173–180 (2018). doi: 10.1021/acsaem.7b00054
- H. Lind et al., Hydrogen evolution reaction for vacancyordered i-MXenes and the impact of proton absorption into the vacancies. Adv. Sustain. Syst. 5, 2000158 (2020). doi: 10.1002/adsu.202000158
- J. Zhang et al., Single platinum atoms immobilized on an MXene as an efficient catalyst for the hydrogen evolution reaction. Nat. Catal. 1, 985–992 (2018). doi: 10.1038/ s41929-018-0195-1
- T. Y. Ma, J. L. Cao, M. Jaroniec, S. Z. Qiao, Interacting carbon nitride and titanium carbide nanosheets for high-performance oxygen evolution. *Angew. Chem. Int. Ed.* 55, 1138–1142 (2016). doi: 10.1002/anie.201509758; pmid: 26629779
- Y. Luo et al., Efficient electrocatalytic N₂ fixation with MXene under ambient conditions. Joule 3, 279–289 (2019). doi: 10.1016/j.joule.2018.09.011
- A. M. Jastrzębska et al., In vitro studies on cytotoxicity of delaminated Ti₃C₂ MXene. J. Hazard. Mater. 339, 1–8 (2017). doi: 10.1016/j.jhazmat.2017.06.004; pmid: 28601597
- 136. H. Lin, S. Gao, C. Dai, Y. Chen, J. Shi, A two-dimensional biodegradable niobium carbide (MXene) for photothermal tumor eradication in NIR-I and NIR-II biowindows. J. Am. Chem. Soc. 139, 16235–16247 (2017). doi: 10.1021/ jacs.7b07818; pmid: 29063760

- H. Lin, Y. Wang, S. Gao, Y. Chen, J. Shi, Theranostic 2D tantalum carbide (MXene). Adv. Mater. 30, 1703284 (2018). doi: 10.1002/adma.201703284: pmid: 29226386
- Z. Li et al., Surface nanopore engineering of 2D MXenes for targeted and synergistic multitherapies of hepatocellular carcinoma. Adv. Mater. 30, e1706981 (2018). doi: 10.1002/ adma.201706981; pmid: 29663543
- K. Rasool et al., Antibacterial activity of Ti₃C₂T_x MXene. ACS Nano 10, 3674–3684 (2016). doi: 10.1021/acsnano.6b00181; pmid: 26909865
- 140. N. Driscoll et al., Two-dimensional Ti₃C₂ MXene for highresolution neural interfaces. ACS Nano 12, 10419–10429 (2018). doi: 10.1021/acsnano.8b06014; pmid: 30207690
- 141. B. B. Murphy et al., A gel-free Ti₃C₂T_x-based electrode array for high-density, high-resolution surface electromyography. Adv. Mater. Technol. 5, 2000325 (2020). doi: 10.1002/ admt.202000325; pmid: 33693054
- 142. E. J. Ward et al., 2D titanium carbide (Ti₃C₂T_x) in accommodating intraocular lens design. Adv. Funct. Mater. 30, 2000841 (2020). doi: 10.1002/adfm.202000841
- 143. F. Meng et al., MXene sorbents for removal of urea from dialysate: A step toward the wearable artificial kidney. ACS Nano 12, 10518–10528 (2018). doi: 10.1021/ acsnano.8b06494; pmid: 30257087
- 144. Q. Zhao et al., Adsorption of uremic toxins using Ti₃C₂T_x MXene for dialysate regeneration. ACS Nano 14, 11787–11798 (2020). doi: 10.1021/acsnano.0c04546; pmid: 32830949
- 145. X. Sang et al., In situ atomistic insight into the growth mechanisms of single layer 2D transition metal carbides. Nat. Commun. 9, 2266 (2018). doi: 10.1038/ s41467-018-04610-0; pmid: 29891836
- 146. G. Deysher et al., Synthesis of Mo₄VAlC₄ MAX phase and two-dimensional Mo₄VC₄ MXene with five atomic layers of transition metals. ACS Nano 14, 204–217 (2020). doi: 10.1021/acsnano.9b07708; pmid: 31804797
- 147. C. Xu et al., Large-area high-quality 2D ultrathin Mo₂C superconducting crystals. Nat. Mater. 14, 1135–1141 (2015). doi: 10.1038/nmat4374; pmid: 26280223
- 148. P. Urbankowski et al., 2D molybdenum and vanadium nitrides synthesized by ammoniation of 2D transition metal carbides (MXenes). Nanoscale 9, 17722–17730 (2017). doi: 10.1039/ C7NR06721F; pmid: 29134998
- J. Cao et al., Realization of 2D crystalline metal nitrides via selective atomic substitution. Sci. Adv. 6, eaax8784 (2020). doi: 10.1126/sciadv.aax8784; pmid: 31950078
- T. Zhao, S. Zhang, Y. Guo, Q. Wang, TiC₂: A new twodimensional sheet beyond MXenes. *Nanoscale* 8, 233–242 (2016). doi: 10.1039/C5NR04472C; pmid: 26503155

- L. T. Alameda, P. Moradifar, Z. P. Metzger, N. Alem, R. E. Schaak, Topochemical deintercalation of Al from MoAIB: Stepwise etching pathway, layered intergrowth structures, and two-dimensional MBene. J. Am. Chem. Soc. 140, 8833–8840 (2018). doi: 10.1021/jacs.8b04705; pmid: 29906120
- L. T. Alameda, C. F. Holder, J. L. Fenton, R. E. Schaak, Partial etching of Al from MoAlB single crystals to expose catalytically active basal planes for the hydrogen evolution reaction. *Chem. Mater.* 29, 8953–8957 (2017). doi: 10.1021/ acs.chemmater.7b02511
- Y. Yu, J. Zhou, Z. Sun, Novel 2D transition-metal carbides: Ultrahigh performance electrocatalysts for overall water splitting and oxygen reduction. Adv. Funct. Mater. 30, 2000570 (2020). doi: 10.1002/adfm.202000570
- M. Khazaei et al., Novel MAB phases and insights into their exfoliation into 2D MBenes. Nanoscale 11, 11305–11314 (2019). doi: 10.1039/C9NR01267B; pmid: 31165851
- 155. H. Kumar et al., Tunable magnetism and transport properties in nitride MXenes. ACS Nano 11, 7648–7655 (2017). doi: 10.1021/acsnano.7b02578; pmid: 28558192
- 156. M. Khazaei, A. Ranjbar, M. Arai, S. Yunoki, Topological insulators in the ordered double transition metals M₂/M^{*}C₂ MXenes (M'= Mo, W; M"=Ti, Zr, Hf). Phys. Rev. B 94, 125152 (2016). doi: 10.1103/PhysRevB.94.125152
- H. Weng et al., Large-gap two-dimensional topological insulator in oxygen functionalized MXene. Phys. Rev. B 92, 075436 (2015). doi: 10.1103/PhysRevB.92.075436
- N. Xu et al., Zero-dimensional MXene-based optical devices for ultrafast and ultranarrow photonics applications. Adv. Sci. 7, 2002209 (2020). doi: 10.1002/advs.202002209; pmid: 33240766
- Y. I. Jhon et al., Metallic MXene saturable absorber for femtosecond mode-locked lasers. Adv. Mater. 29, 1702496 (2017). doi: 10.1002/adma.201702496; pmid: 28714145
- K. Rasool et al., Water treatment and environmental remediation applications of two-dimensional metal carbides (MXenes). Mater. Today 30, 80–102 (2019). doi: 10.1016/ j.mattod.2019.05.017
- V. Kamysbayev et al., Colloidal gelation in liquid metals enables functional nanocomposites of 2D metal carbides (MXenes) and lightweight metals. ACS Nano 13, 12415–12424 (2019). doi: 10.1021/acsnano.9b06207; pmid: 31560851
- J. Guo et al., Cold sintered ceramic nanocomposites of 2D MXene and zinc oxide. Adv. Mater. 30, e1801846 (2018). doi: 10.1002/adma.201801846; pmid: 29944178
- 163. F. Bian, L. Sun, L. Cai, Y. Wang, Y. Zhao, Bioinspired MXene-integrated colloidal crystal arrays for multichannel bioinformation coding. Proc. Natl. Acad. Sci. U.S.A. 117,

- 22736–22742 (2020). doi: 10.1073/pnas.2011660117; pmid: 32868413
- 164. B. Lyu et al., 2D MXene-TiO₂ core-shell nanosheets as a data-storage medium in memory devices. Adv. Mater. 32, e1907633 (2020). doi: 10.1002/adma.201907633; pmid: 32187736
- H. Wei et al., Redox MXene artificial synapse with bidirectional plasticity and hypersensitive responsibility. Adv. Funct. Mater. 31, 2007232 (2021). doi: 10.1002/ adfm.202007232
- 166. C. E. Shuck et al., Scalable synthesis of Ti₃C₂T_x MXene. Adv. Eng. Mater. 22, 1901241 (2020). doi: 10.1002/ adem.201901241
- S. Uzun et al., Additive-free aqueous MXene inks for thermal inkjet printing on textiles. Small 17, 2006376 (2021). doi: 10.1002/smll.202006376
- J. Lipton et al., Scalable, highly conductive, and micropatternable MXene films for enhanced electromagnetic interference shielding. Matter 3, 546–557 (2020). doi: 10.1016/j.matt.2020.05.023
- B. Xu et al., Ultrathin MXene-micropattern-based field-effect transistor for probing neural activity. Adv. Mater. 28, 3333–3339 (2016). doi: 10.1002/adma.201504657; pmid: 26924616
- A. Levitt et al., 3D knitted energy storage textiles using MXene-coated yarns. Mater. Today 34, 17–29 (2020). doi: 10.1016/j.mattod.2020.02.005
- H. Lin, X. Wang, L. Yu, Y. Chen, J. Shi, Two-dimensional ultrathin MXene ceramic nanosheets for photothermal conversion. *Nano Lett.* 17, 384–391 (2017). doi: 10.1021/ acs.nanolett.6b04339; pmid: 28026960

ACKNOWLEDGMENTS

Funding: Y.G. and A.V.M. acknowledge support from the Fluid Interface Reactions, Structures, and Transport (FIRST) Center, an Energy Frontier Research Center funded by the US Department of Energy, Office of Science, and Office of Basic Energy Sciences for MXene electrochemistry research. Search for new MXene compositions by Y.G. was also supported by National Science Foundation awards DMR-2041050 and DMR-2035007. J.R. acknowledges funding from the Knut and Alice Wallenberg (KAW) Foundation and the Swedish Foundation for Strategic Research (SSF). The Swedish Government Strategic Research Area in Materials Science on Functional Materials at Linköping University (Faculty Grant SFO Mat LiU No. 2009 00971) is also acknowledged. Competing interests: None declared.

10.1126/science.abf1581



The world of two-dimensional carbides and nitrides (MXenes)

Armin VahidMohammadi, Johanna Rosen and Yury Gogotsi

Science **372** (6547), eabf1581. DOI: 10.1126/science.abf1581

A family of thin materials

Two-dimensional (2D) materials have attracted interest because of the unusual properties that emerge in these confined structures. There is a growing family of 2D metal carbides and nitrides known as MXenes that contain an odd number of layers in which metals (M) sandwich carbon or nitrogen (X) layers. VahidMohammadi *et al.* reviewed the progress in synthesizing this growing library of materials. Mixed-metal combinations can be used, as well as a range of surface terminations, making it possible to tune the properties. However, there are still challenges in improving the synthesis methods and developing techniques that can be scaled up.

Science, abf1581**, this issue p. eabf1581**

ARTICLE TOOLS http://science.sciencemag.org/content/372/6547/eabf1581

REFERENCES This article cites 169 articles, 13 of which you can access for free

http://science.sciencemag.org/content/372/6547/eabf1581#BIBL

PERMISSIONS http://www.sciencemag.org/help/reprints-and-permissions

Use of this article is subject to the Terms of Service